Main Manuscript for

Sugar Signaling Induces Dynamic Changes During Meristem Development to Regulate Flowering in Arabidopsis

Magdalena Musialak-Lange[1], Katharina Fiddeke[1,#], Annika Franke[1,#], Friedrich Kragler[1], Christin Abel[1], and Vanessa Wahl[1,*]

Affiliations: [1]Max Planck Institute of Molecular Plant Physiology, Department of Metabolic Networks, Am Mühlenberg 1, Potsdam, 14476, Germany.

[#]K.F. and A.F. contributed equally

[*]**Correspondence**: Vanessa Wahl

Email: vanessa.wahl@mpimp-golm.mpg.de

Abstract

Aerial parts of plants originate from pluripotent stem cells in the shoot apical meristem. Their population is maintained via the maintenance regulators *WUSCHEL* and *CLAVATA3* in a negative feed-back loop. Meristem size is dynamic and undergoes a more than 2-fold expansion upon the transition to reproductive growth. The mechanism controlling this doming is largely unknown, but coinciding increased trehalose 6-phosphate and changed meristem size in overexpressing or knockdown lines of *TREHALOSE PHOSPHATE SYNTHASE1* suggest a participation of sugar signaling. Here we show that *TREHALOSE PHOSPHATE PHOSPHATASEJ* is directly regulated by WUSCHEL. Plants with reduced levels of *TREHALOSE PHOSPHATE PHOSPHATASEJ* in the outer meristem layer are flowering early and its reduction in the late flowering *clavata3* mutant, restores wild-type flowering. This is caused by a reduction of mature miR156 and increased expression of *SQUAMOSA PROMOTER-BINDING PROTEIN-LIKE* genes. We demonstrate that these are important for age pathway-induced flowering, in a negative feed-back loop with WUSCHEL downstream of the trehalose 6-phosphate pathway. In summary, our findings demonstrate a dynamic feed-back regulation between central maintenance and flowering time regulators with sugar signaling.

Keywords: flowering / meristem maintenance / sugar / Trehalose 6-phosphate (T6P) pathway / WUS

Introduction

All above ground plant organs such as leaves and flowers originate from the shoot apical meristem (SAM). The *Arabidopsis thaliana* (Arabidopsis) SAM is organized in three clonally distinct cell layers: the outer mono cell layers, L1 and L2, and the several cell files comprising L3. Functionally, the SAM consist of a central zone (CZ), containing undifferentiated cells with a self-renewing potential, an organizing centre (OC), inducing and maintaining an adequate number of cells in the CZ, a peripheral zone (PZ) which receives cells from the CZ that are differentiating and incorporated into leaf or flower primordia, and a rib zone (RZ) producing the stem (Pfeiffer *et al*, 2017). Communicating position-dependent properties among cells within and between the different zones is crucial for SAM function. Two non-cell autonomously acting factors regulate each other in a negative feed-back loop. The homeodomain transcription factor *WUSCHEL* (*WUS*) is expressed in the OC, and the signalling peptide *CLAVATA3* (*CLV3*) in the CZ. Thus, mobile WUS transcription factor, secreted from the OC, activates expression of *CLV3* in the CZ above, while CLV3 peptide restricts the *WUS* expression domain to the OC. Hence, *WUS* and *CLV3* expression domains are considered mutually exclusive and their negative feed-back regulation as very robust, which can only be modulated within tight limits (Pfeiffer *et al.*, 2017).

Development as a whole and SAM maintenance in particular demands continuous cross talk between its regulatory processes and the available resources. SAM maintenance and flowering time are important determinants of crop yield. During floral transition cell division is activated and the SAM undergoes a dramatic increase in size known as doming (Jacqmard *et al*, 2003; Kwiatkowska, 2008) (Figure 1A) and marks the time between the vegetative stage (production of leaves) and the reproductive stage (formation of flowers). Since this transition requires a massive reorganization of organ development and sufficient energy, it is tightly controlled by environmental conditions and availability of nutrients (Andres & Coupland, 2012; Olas *et al*, 2019; Ponnu *et al*, 2020; Srikanth & Schmid, 2011; Wahl *et al*, 2013). Only recently the early cellular changes were associated with floral regulators that control GA biosynthesis (Kinoshita *et al*, 2020). However, the knowledge on the mechanisms controlling doming is still scarce.

In plants, the sugar phosphate, trehalose 6-phosphate (T6P), it is synthetized from UDP-glucose and glucose 6-phosphate via TREHALOSE PHOSPHATE SYNTHASE (TPS) and is converted to trehalose by TREHALOSE PHOSPHATE PHOSPHATESES (TPP) (Fichtner & Lunn, 2021). T6P serves as a signal for sucrose availability, which is conveyed to downstream metabolic and growth responses through still largely unknown mechanisms (Fichtner & Lunn, 2021). In Arabidopsis sugar signalling affects the vegetative phase change, the transition between the formation of juvenile and adult leaves, via the T6P pathway (Ponnu *et al.*, 2020; Yang *et al*, 2013; Yu *et al*, 2013). In addition, the T6P pathway is involved in shoot branching (Fichtner *et al*, 2020), and induces flowering via regulating key flowering genes in leaves and at the SAM (Wahl *et al.*,

2013). In leaves, *TPS1*, coding for the T6P synthesizing enzyme, is necessary and sufficient to induce *FLOWERING LOCUS T* (*FT*), the florigen, connecting the photoperiod signal with a physiological signal. In addition, the T6P pathway affects the age-dependent microRNA156 (miR156)/*SQUAMOSA PROMOTER-BINDING PROTEIN-LIKE* (*SPL*) module at the SAM (Wahl *et al.*, 2013). Increased T6P levels coincide with doming (Wahl *et al.*, 2013), and a spatial change of the *WUS* expression domain. This suggests a participation of sugar signaling in regulating SAM dynamics through transient uncoupling of the negative feed-back regulation between WUS and CLV3. Here we show that WUS directly regulates *TPPJ*. A late flowering phenotype of *clv3* is caused by increased levels of mature miR156 and decreased expression of *SPL* genes and is restored when *TPPJ* is downregulated in the outer meristem layer. We further demonstrate a negative feed-back loop with WUS and SPL4 downstream of the T6P pathway. In summary, we provide evidence for a dynamic feed-back regulation between central meristem maintenance and flowering time regulators with sugar signaling.

Results and Discussion

The T6P pathway affects SAM size. To assess whether the morphological changes at the transition SAM (Figure 1A) involve the T6P pathway, we investigated the effect on SAM architecture by decreasing *TPS1* by the means of an artificial microRNA in the SAM proper (*35S:amiRTPS1*; Figure S1) and increasing *TPS1* in the CZ (*CLV3:TPS1*, Figure S2). These plants have smaller and bigger vegetative and reproductive meristems (Figure 1B,C), resulting in smaller and bigger plants, respectively (Wahl *et al.*, 2013).

TPS1 knock-out mutants are embryo lethal, likely as a result of insufficient cell cycle activity at torpedo stage of embryogenesis (Gómez *et al*, 2006). Cell cycle genes were also found to be highly induced at transition to flowering (Klepikova *et al*, 2015) confirming earlier findings (Jacqmard *et al.*, 2003). In order to test, whether cell proliferation is the cause of the effect observed downstream of the T6P pathway, we used specific probes against transcripts of *HISTONE4, CYCLIN D3;1* and *CYCLIN-DEPENDENT KINASE2;1*, three cell cycle marker genes, for RNA *in situ* hybridization on longitudinal sections through the SAM (Figure S3). The results show more abundant staining indicating the three cell cycle marker genes in the presence of elevated T6P levels and less staining, when T6P levels were reduced. This suggests a higher proliferation rate and an increased number of cells produced to adopt organ-specific cell fates at the periphery as a plausible reason for decreased SAM size of *TPS1* overexpression and *vice versa* increased SAM size of *TPS1* knock-down lines (Figure 1B,C).

69 **Spatial changes of *WUS* expression in a transition SAM**. In line with these findings, the floral
70 transition coincides with increased T6P levels (Wahl *et al.*, 2013). To assess whether this is
71 related to *WUS* or *CLV3* expression in a wild-type SAM, we analyzed their expression in a time
72 series spanning floral transition (Figure 1D). Throughout the vegetative phase SAM size gradually
73 increases due to rising cell numbers (Figures 1A, S4) (Kinoshita *et al.*, 2020), reaching its
74 maximum at floral transition, independent of whether the plants are grown in long days (LD)
75 (Figure 1A) or in short days (SD) followed by a transfer to LD (Figure S5). An enlarging SAM at
76 floral transition correlates with a larger *WUS* expression domain expanding into the CZ and the
77 outer cell layer (L1) (Figure 1D-F).

78 Cytokinin signaling was previously reported to respond to carbon in seedlings (Leibfried *et al*,
79 2005; Pfeiffer *et al*, 2016; Snipes *et al*, 2018). Its transient occurrence in L1 may thus explain the
80 presence of *WUS* transcript in the outer SAM layers. However, cytokinin levels are not altered in
81 L1 cells as indicated by the synthetic cytokinin reporter *TCSn:GFP* (Zurcher *et al*, 2013) (Figure
82 S6). Further, while *WUS* expands to L1 for a short period (8-10 DAG), the *CLV3* expression
83 domain remains expanded post floral transition (Figure 1D,G). This suggests a transient
84 uncoupling of the negative feed-back regulation between WUS and CLV3, which is re-established
85 at the reproductive SAM (16 DAG), resembling earlier vegetative SAM expression patterns (6
86 DAG) (Figure 1D).

87 ***TPPJ* is directly regulated by WUS**. To understand how the T6P pathway might control this
88 process, we first analyzed expression of the ten genes encoding TREHALOSE PHOSPHATE
89 PHOSPHATASEs (TPP) (Fichtner & Lunn, 2021). Except for *TPPC* and *TPPD*, which are
90 expressed below detection limit of RNA *in situ* hybridization, we found that all are expressed in
91 distinct SAM domains (Figure S7). *TPPJ* strongly increases in the enlarged SAM of *clv3-7* due to
92 an ectopic expression in L1 and L2 (Figures 2A-C; S8, S9). Notably, in *clv3-7* and *clv3-10*
93 mutants high levels of *WUS* in the outer SAM layers (Brand *et al*, 2000) coincide with ectopic
94 expression of *TPPJ* (Figure S9), while *TPPJ* is repressed in a *wus-7* background (Figure S10A).
95 In addition, a previously published data set shows induced levels of *TPPJ* upon DEX induced
96 expression of *WUS* in a *35S:WUS-GR* line (Busch *et al*, 2010) (Figure S10 B). To assess whether
97 ectopic expression of *TPPJ* contributes to the enlarged SAM of the *clv3* mutant, we
98 overexpressed *TPPJ* in the wild type (*35S:TPPJ*; Figure 2D,E), which resulted in plants with
99 significantly enlarged SAMs (Figure 2F).

100 These results imply a direct influence of WUS on *TPPJ*, and is supported by an *in silico* analysis
101 which predicts multiple, canonical WUS binding sites in the sequence upstream of *TPPJ*
102 ($TPPJ^{WUS}$; Figure 3A) (Leibfried *et al.*, 2005; Lohmann *et al*, 2001; Sloan *et al*, 2020; Yadav *et al*,
103 2011). To understand if WUS directly controls *TPPJ*, we performed *in vivo* transactivation assays.

104 These show that WUS activates reporter gene expression when using a 2865bp 5'*TPPJ*
105 sequence, containing 17 putative *TPPJ*^{WUS} sites (Figure 3A). Progressive deletion of this
106 sequence results in a reduction of reporter gene activation, suggesting an additive effect of the
107 individual *TPPJ*^{WUS} sites (#1-6; Figure 3A,B). We confirmed direct binding of WUS to three
108 distinct regions of the *TPPJ* promoter (I, II, and III; Figures 3C-E; S11) by chromatin
109 immunoprecipitation (ChIP) coupled to PCR using a specific antibody against WUS (Figures S11,
110 S12), while all other regions did not indicate binding (Figures S11, S13). We observed enrichment
111 of WUS binding to *TPPJ*^{WUS} sites up to 0.67% of the input DNA in *clv3-7* and 0.75% of the input
112 DNA in *clv3-10* apices, both of which express *WUS* at high levels in comparison to input DNA
113 from wild-type apices, where *WUS* is expressed in only a few cells and input DNA from leaves,
114 with no WUS (Figures 3C-E; S10). Electrophoretic mobility shift assays (EMSA) confirm specific
115 *in vitro* binding of WUS to the investigated sequences (I, II 1-3, III 1-3; Figure 3F; S14). In
116 summary, we demonstrate that seven out of 17 putative *TPPJ*^{WUS} sites are directly targeted by
117 WUS *in vivo*.

118 **TPPJ controls flowering from the outer SAM layer**. A *tppj* mutant with a T-DNA insertion in the
119 6th exon, which specifically knocks-out *TPPJ* expression (Figure S15), flowers significantly earlier
120 than the wild type (Table S1). To further assess the role of *TPPJ* at the SAM we used an artificial
121 miRNA (amiR) approach to downregulate *TPPJ* (*35S:amiRTPPJ*; Figure S16)(Schwab *et al*,
122 2006). Plants overexpressing either of two versions of an *amiRTPPJ* (V1, V2) flower significantly
123 earlier in LD and SD (Figure S17; Table S1). *ML1* expression specifically and stably localizes to
124 L1 in all investigated stages (Figure S18). *ML1:amiRTPPJ* reduces *TPPJ* expression in L1
125 (Figure S19), has a smaller SAM and flowers significantly earlier in LD and SD (Figures 4A,B;
126 S20, S21; Table S1), while the level of *TPPJ* reduction is proportional to the acceleration of
127 flowering (Figures 4B,C; S16; Table S1).

128 To date there are no reports that mutants in meristem maintenance genes have a flowering
129 phenotype. We found that *clv3* plants are late flowering (Figure 4C; Table S1). However, when
130 *ML1:amiRTPPJ* is introgressed into the *clv3-7* or *clv3-10* background, the late flowering
131 phenotype is restored to wild-type (Figures 4C; S21; Table S1), suggesting that *TPPJ* expression
132 in the outer meristem layers is causal for the late flowering phenotype of *clv3*. Hence, the early
133 flowering of *ML1:amiRTPPJ* in a wild-type background is due to a reduction of *TPPJ* expression
134 in the outer meristem layer in its endogenous expression domain. In addition, other prominent
135 morphological defects of *clv3-10* such as the fasciated stem and enormous inflorescence SAM
136 are visibly reduced in the presence of *ML1:amiRTPPJ* (Figure S21).

137 **WUS regulates the age pathway through *SPL4***. We previously reported that the T6P pathway
138 influences the age pathway at the SAM (Wahl *et al.*, 2013). We therefore next analyzed mature

139 miR156, as well as the expression of *SPL3*, *SPL4*, *SPL5*, *SPL9* and *SPL15*, all associated with
140 floral transition in one or the other way (Hyun *et al*, 2017; Xie *et al*, 2020). We found a strong
141 reduction of mature miR156 levels correlating with decreased *TPPJ* in *ML1:amiRTPPJ*, and
142 corresponding increased expression of *SPL3, SPL4, SPL5*, and *SPL9* (Figure 4D). In line,
143 miR156 was more abundant in *35S:TPPJ*, while the corresponding *SPL*s were downregulated
144 (Figure 4D). Expression of *SPL15*, previously described as an important integrator of plant age
145 into the regulation of floral onset in SD (Hyun *et al*, 2016; Wang *et al*, 2009; Yamaguchi *et al*,
146 2014), was not differentially expressed in the transgenic lines (Figure S22A).

147 Uncoupling of the WUS/CLV3 feed-back loop occurs downstream of the T6P pathway and
148 involves age pathway components. Interestingly, a study by Fouracre and Poethig indicates an
149 active pool of miR156 in the SAM, which is essential for early shoot maturation and affects leaf
150 identity. In addition, apices of a *wus-5* mutant had decreased miR156 levels and increased *SPL9*
151 expression, although expression of none of the other SPLs was tested. However, plants with
152 increased miR156 (*35S:miR156a*) have a larger SAM, while those with reduced miR156
153 (quadruple *mir156a,c,mir157a,c*) have a smaller SAM, and a sextuple *spl2,9,10,11,13,15*
154 increased SAM size. This is accompanied with an increased *WUS* expression in the sextuple
155 mutant, suggesting the potential repression of *WUS* by any or all of the *SPL*s mutated in hextuple
156 plants (Fouracre & Poethig, 2019). Notably, we found miR156 levels significantly increased in
157 *clv3-10* apices (Figure 5A). In response, *SPL3*, *SPL5*, and *SPL9* were reduced supporting the
158 late flowering phenotype of the mutant, while *SPL15* was not affected (Figure S22B). In contrast
159 to what would be expected, we found more *SPL4* transcript in apices of the late flowering *clv3-10*
160 (Figure 5A).

161 The contribution of SPL9 and SPL15 to the regulation of the floral onset is well established (Hyun
162 *et al.*, 2016; Wang *et al.*, 2009; Yamaguchi *et al.*, 2014), but there is some dispute about whether
163 or not SPL3, SPL4, and SPL5 are important. While overexpression of *SPL3, SPL4*, and *SPL5*
164 induces flowering (Jung *et al*, 2016; Wu & Poethig, 2006), a triple T-DNA insertion mutant was
165 previously reported to not display any flowering phenotype (Xu *et al*, 2016). However, a recent
166 study analyzed a triple deletion mutant generated by CRISPR/*Cas9* in relation to light signaling
167 and also reported on a delay in flowering time (Xie *et al.*, 2020). Similarly, we generated individual
168 deletion mutants in the respective SPLs using CRISPR/*Cas9* (Figure S23). As compared to single
169 *spl* mutant and wild-type plants, higher order *spl3*, *spl4* and *spl5* deletion mutants are significantly
170 later flowering in all lines with *spl4* (Figure 5B-D; Table S1). This argues for an important role of
171 *SPL4* in inducing flowering. *SPL4*, similar to *SPL3* and *SPL5,* is induced at the wild-type SAM at
172 floral transition (Schmid *et al*, 2003). It is expressed in the center of the SAM, in a domain
173 overlapping with the WUS protein, while *SPL3*, *SPL5*, *SPL9*, and *SPL15* are expressed at the
174 periphery of the SAM and in the vasculature of young leaves (Daum *et al*, 2014; Hyun *et al.*,

175 2016; Olas *et al.*, 2019; Wang *et al.*, 2009; Yadav *et al.*, 2011). This denotes a direct regulation of
176 *SPL4* by WUS, which would explain increased *SPL4* levels in the *clv3* mutant (Figure 5A) and the
177 previously identified partial miR156-dependent regulation of the *SPL*s by the T6P pathway (Wahl
178 *et al.*, 2013). Indeed, we observed reduced expression of *SPL4* in *wus-7* apices, a weak allele
179 with a mutation in the WUS DNA binding domain resulting in smaller but maintained SAM tissue
180 (Graf *et al*, 2010; Lin *et al*, 2016). In contrast, none of the other *SPL*s were reduced (Figures 5E;
181 S22C) and miR156 levels did not change (Figure 5E). This is unexpected as a recent publication
182 demonstrated decreased miR156 levels and increased *SPL9* expression in apices of a *wus-5*
183 mutant (Fouracre & Poethig, 2019). *wus-5* is however a strong *wus* null allele with very little
184 residual SAM tissue (McElver *et al*, 2001; Sonoda *et al*, 2007), which might explain the difference.
185 We identified a larger number of potential *SPL4*^{WUS} sites when compared to the other *SPL*s
186 (Figures 5F; S24). A transactivation assay demonstrated induction of the luciferase reporter
187 coupled to 5'*SPL4* sequences by WUS, with the shortest fragment covering most of the inductive
188 effect (Figure 5G). This sequence contains five *SPL4*^{WUS} sites, four of which could be separately
189 tested by ChIP-PCR. This indeed confirmed direct induction of *SPL4* by WUS (Figures 5H; S25).
190 However, these results also suggest that additional players downstream of the WUS/CLV3 feed-
191 back loop are important for the onset of flowering, which cannot be bypassed by an otherwise
192 inductive SPL4 (Figure 5A).

193 **A feed-back regulation between the T6P pathway and WUS involves the age pathway**. An
194 enlarging SAM at floral transition correlates with a larger *WUS* expression domain expanding into
195 the CZ and the outer cell layer (L1) (Figure 1D-F). Interestingly, we found reduced *TPS1* levels
196 (*35S:amiRTPS1*) lead to an enlarged OC domain marked by *WUS* (Figure 6A) that overlaps with
197 the CZ, marked by *CLV3* expression (Figure 6A). Plants overexpressing *TPS1* (*35S:TPS1*, Figure
198 S2) display an increased stem cell pool with otherwise little effect on *WUS* expression (Figure
199 6A). The size of the CZ decreases when expressing *TPS1* under the *CLV3* promoter (Figures 6A;
200 S2), indicating a smaller stem cell pool in support of a much smaller SAM size of the very early
201 flowering *CLV3:TPS1* (Wahl *et al.*, 2013).
202 *TPPJ* overexpression results in significantly enlarged SAMs (Figure 2F), and importantly,
203 expands *WUS* expression into the outer SAM layers, while *CLV3* expression seems to be little
204 affected (Figure 6B,C). Consistent with this, *CLV3* expression increases to much higher levels in
205 *ML1:amiRTPPJ* (Figure 6C), suggesting an active role of the T6P pathway in the outer meristem
206 layer regarding stem cell maintenance. In addition, *WUS* is induced (Figures 6C-D), indicating
207 uncoupling of the WUS/CLV3 feed-back loop downstream of the T6P pathway.
208 We next investigate whether this is in part due to the function of the age pathway downstream of
209 the T6P pathway. While we found *WUS* to be induced (Figure S26A,B), its expression seems to
210 be reduced in the CZ in the transition SAM of all but *spl3,5* mutant SAMs (Figure S26A). This

211 cannot be explained by an altered expression of *CLV3*, as we found it generally slightly reduced
212 in all mutant lines (Figure S26C,D).
213 Since *WUS* and *SPL4* expression domains are largely overlapping (Daum *et al.*, 2014; Olas *et al.*,
214 2019; Torti *et al*, 2012; Yadav *et al.*, 2011), we asked whether a feed-back loop, involving direct
215 regulation of *WUS* by SPL4, would explain the observed expression patterns. We identified one
216 WUS^{SPL4} site -1067bp upstream of the *WUS* coding sequence (Figure 6E). SPL4 significantly and
217 specifically reduced reporter gene expression in an Arabidopsis protoplast-based transactivation
218 assay, indicating that it can repress *WUS in vivo* (Figure 6F,G). EMSA confirmed this result
219 (Figure 6H). This finding is supported by a promoter study analyzing a series of deletion
220 constructs of the 5'*WUS* sequence (Baurle & Laux, 2005). Among them one which deleted a
221 sequence including the WUS^{SPL4} site (Δ4, -941/-604 from transcription start site; -1067/-730
222 upstream of coding sequence). Importantly, this deletion construct led to a stronger activation
223 while others rather led to a reduction of a GUS reporter, especially when affecting the sequences
224 close to the transcription start site. This indicates the loss of regulatory sequences which are
225 targeted by repressors of WUS such as SPL4 (Baurle & Laux, 2005). Taken together, our results
226 demonstrate a likely transient negative feed-back regulation between SPL4 and WUS.

227 **Conclusion**

228 Taken together, we unraveled dynamic feed-back regulations between sugar signaling, central
229 meristem maintenance and flowering time regulators that coordinate cell proliferation and
230 metabolism, providing the basis and energy necessary for doming during floral transition.

231 Proliferation, self-renewal and differentiation of cells originating from stem cells are the basis for
232 the plants' remarkable plasticity. Stem cell systems are formed during embryogenesis. The SAM
233 as primary meristem is retained stably throughout plant development (Pfeiffer *et al.*, 2017). The
234 initiation of reproductive growth marks a very prominent change in a plant's morphology and
235 requires large-scale reorganization of SAM architecture and sink-source relationships within all
236 flowering plants. Within cells, sucrose is an important basis for energy production and biomass.
237 To prevent starvation, energy-demanding developmental transitions are tightly coordinated with
238 endogenous sucrose availability through intricate signaling systems (Fernie *et al*, 2020). The
239 sucrose signaling T6P pathway was previously found to impact on cell cycle regulators (Gómez *et*
240 *al.*, 2006). These were also demonstrated as differentially expressed at the transition stage
241 (Klepikova *et al.*, 2015).

242 We show that in Arabidopsis the negative feed-back loop between the central meristem
243 maintenance regulators WUS and CLV3, considered as stable until now, uncouples during floral
244 transition. As a result, the *WUS* expression domain is no longer fixed in the center of the SAM but

245 stretches into the outer meristem layers demonstrating unreported OC dynamics. WUS directly
246 regulates *TPPJ*, a component of the T6P pathway, which has an impact on SAM size and thus
247 seems important for cell proliferation and doming of the SAM during the transition phase. Notably,
248 organ production is stalled when *WUS* is ectopically expressed from a *CLV3* promoter into the
249 stem cell niche, and correlates with massive proliferation of meristematic cells (Brand *et al*, 2002).

250 Although *TPPJ* is expressed at the rim of the PZ, it can be activated by WUS *in vivo*, requiring the
251 cell non-autonomous function of a mobile WUS (Daum *et al.*, 2014; Yadav *et al.*, 2011). The fact
252 that WUS does not activate *TPPJ* outside of this domain suggests other factors repressing it in
253 the center of the SAM. These factors are clearly still active in a *clv3* mutant background, where
254 the activation of *TPPJ* by WUS is restricted to the outer SAM layers, suggesting factors outside of
255 this central regulation of the meristem maintenance network (Pfeiffer *et al.*, 2017). It will be
256 interesting to learn more about its regulation in the future.

257 We demonstrate that SPL4, which is expressed in a domain overlapping with the central *WUS*
258 expression domain, directly and negatively regulates *WUS.* In turn, WUS activates *SPL4* in a
259 likely transient negative feed-back regulation, which we suggest to balance sugar-signaling-
260 dependent effects on meristem maintenance at transition. In addition, WUS might repress *SPL5*,
261 as we found slightly but significantly increased expression in *wus-7* apices (Figure 5E). Although
262 they don't seem to respond in a WUS-dependent manner, it remains to be determined whether
263 those SPLs expressed in the periphery of the SAM (SPL3, SPL5 and SPL9) are mobile and
264 therefore independently report on the sucrose status to the central region of the SAM. We
265 suggest that the combined action of the T6P pathway and SPLs expressed at the SAM
266 determines the duration of the doming phase.

267 An important next step will be to understand how SnRK1 and TOR signaling (Baena-González &
268 Lunn, 2020; Caldana *et al*, 2019; Pfeiffer *et al.*, 2016) fit into the emerging picture of the
269 mechanisms regulating floral transition in the future. Apart from the regulation of flowering time
270 (Wahl *et al.*, 2013), it is interesting that the T6P pathway also influences the re-organisation of the
271 SAM during floral transition. Given the ubiquitous nature of carbohydrate signaling and the large-
272 scale change in sink-source relationships within plants (Fernie *et al.*, 2020), it will be interesting to
273 determine if this regulatory mechanism is widely present in the plant kingdom.

274 **Materials and Methods**

275 Plant material and growth conditions

276 All Arabidopsis plants were of the Columbia accession (Col-0), except for *wus-7*, which is in
277 the Ler background (Graf *et al.*, 2010). *clv3-7* (Wisman *et al*, 1998), *clv3-10* (Forner *et al*, 2015),

278 *35S:amiRTPS1*, *CLV3:TPS1* (Wahl *et al.*, 2013), and *TCSn:GFP* (Zurcher *et al.*, 2013) were
279 described previously. The *tppj* insertion mutant (At5g65140, GABI_215C08) was obtained from
280 the Arabidopsis resource stock center (ABRC). Growth chambers were set to 22°C in LD (16h
281 light/8h dark) or SD (8h dark/16h light) with a light intensity of approximately 160 µmol/m^{-2}s^{-1} and
282 a relative humidity of 60-65%. Synchronized induction of flowering was performed as described
283 (Schmid *et al.*, 2003).

284 Plant phenotyping

285 Flowering time of on average of 20 plants per genotype was scored as days to flowering,
286 when shoots were 0.5cm (bolting), and by the total leaf number (TLN), i.e., the sum of rosette leaf
287 (RLN) and cauline leaf numbers (CLN) (Table S1). Meristem size was measured as the area
288 between two organ primordia under the meristem summit of a longitudinal middle section through
289 at least 10 apices from individual plants using the Fiji software version 2.0.0-rc-69/1.52
290 (Schindelin *et al*, 2012).

291 Generation of transgenic lines

292 Plants were transformed (Clough & Bent, 1998), confirmed by PCR and independent,
293 single-insertion, homozygous T3 plants were used for all studies. Oligonucleotides for cloning and
294 for genotyping are given in Tables S2 and S3, respectively. For *35S:TPPJ* and *35S:TPS1* lines,
295 coding sequences of *TPPJ* (At5g65140) and *TPS1* (At1g78580) were cloned via the Gateway®
296 entry vector *pJLBlue* reverse (Mathieu *et al*, 2007) into a *pGREEN-II*-based destination vector.
297 Artificial microRNAs targeting *TPPJ* (*ML1:amiRTPPJ* V1 and V2, *35S:amiRTPPJ* V1 and V2)
298 were designed with the Web MicroRNA Designer (http://wmd3.weigelworld.org/cgi-
299 bin/webapp.cgi)(Schwab *et al.*, 2006). The *Eco*RI/*Bam*HI fragment was cloned via *pJLBlue*
300 reverse (Mathieu *et al.*, 2007) into a *pGREEN-II*-based destination vector with either the *ML1* or
301 *35S* promoter. *spl3, spl4, spl5* knockout lines were generated with the CRISPR/*Cas9* technology
302 (Ruf *et al*, 2019; Wang *et al*, 2015). The NGG PAM recognition sites were defined using the
303 ATUM webtool (https://www.atum.bio) (Figure S23). The *pJF1033* vector, containing a two single
304 guided RNAs scaffold, was used as a template. *Bsa*I products were cloned into the *pJF1031*
305 binary vector (Ruf *et al.*, 2019). Plants with homozygous deletions were back-crossed to Col-0.
306 Homozygous, *Cas9*-free lines were used to generate all higher order mutant lines.

307 RT-qPCR

308 Total RNA was isolated by a modified phenol/chloroform method using a TRIzol reagent
309 (phenol 38% (v/v), guanidine thiocyanate 0.8M ammonium thiocyanate 0.4M, sodium acetate

310 0.1M pH5.0, glycerol 5% (v/v), EDTA 5mM pH8.0, Na-lauroylsarcosine 0.5% (v/v)), followed by
311 sodium acetate precipitation. Genomic DNA was removed with DNase I RNase-free
312 (Ambion™/Thermo Fisher Scientific, Waltham, Massachusetts, US), and cDNA synthesis carried
313 out using a SuperScript™IV Reverse Transcriptase Kit (Thermo Fisher Scientific, Waltham,
314 Massachusetts, US) according to the instructions. Mature miR156 stem-loop primers (Table S4)
315 were added to the cDNA synthesis reaction (1:1 with oligo dT(18) primer) (Varkonyi-Gasic *et al*,
316 2007).

317 RT-qPCR was performed with the ABI Prism 7900 HT fast real time PCR system (Applied
318 Biosystems/Life Technologies, Darmstadt, Germany) using a Power SYBR® Green-PCR Master
319 Mix (Applied Biosystems/Life Technologies, Darmstadt, Germany) for expression analyses and
320 ChIP-PCRs. Oligos are listed in Table S4 (RT-qPCR) and S5 (ChIP-PCR). For analysis the SDS
321 2.4 software (Applied Biosystems/Life Technologies, Darmstadt, Germany) was used
322 (Czechowski *et al*, 2004). cDNA quality was determined and expression values were calculated
323 (Wahl *et al.*, 2013).

324 RNA *in situ* hybridization

325 Probes were synthesized using the DIG RNA Labeling Kit (Roche, Mannheim, Germany) on
326 CDSs of the target genes cloned into the *pGEM®-T Easy* vector (Promega, Madison, Wisconsin,
327 US). Oligonucleotides and construct IDs are listed in Table S6. Wax embedding, sectioning and
328 RNA *in situ* hybridization, and imaging were performed as described (Wahl *et al.*, 2013).

329 ChIP-PCR

330 For ChIP-PCR, 100 apices or 1.5g leaves per replicate (Col-0, *clv3-7* and *clv3-10*) were
331 fixed in 1% (v/v) formaldehyde buffer (10mM sodium phosphate buffer, pH7; 50mM NaCl; 100mM
332 sucrose) under vacuum. ChIP was performed (Kaufmann *et al*, 2010) with modifications: Antibody
333 incubation (anti-WUS; AS11 1759; Agrisera) was extended o/n at 4°C and Agarose beads
334 (Protein A-Agarose; sc-2001; Santa Cruz Biotechnology) to 6h at 4°C. Immunoprecipitated DNA
335 was analyzed by RT-qPCR. Ct values of *TPPJ* and *SPL4* promoter regions were normalized to
336 the Ct value of a region within the *UBQ10* promoter. The % of enrichment was calculated as
337 relative to expression of the input of the individual regions. ChIP on apices of Col-0, *clv3-7* and
338 *clv3-10* without antibody and ChIP on Col-0, *clv3-7* and *clv3-10* leaves were controls (Figure
339 S10). Note that in contrast to the input no amplification was observed in the controls (Figure S11,
340 S25) and the previously published confirmed WUS target sites were detected (Figure
341 S12)(Leibfried *et al.*, 2005; Yadav *et al.*, 2011). Oligonucleotides are listed in Table S5.

342 Transactivation assay

343 For the effector line, the *WUS* (At2g17950) and *SPL4* (At1g53160) CDS were cloned via the
344 Gateway® entry vector *pJLBlue* reverse (Mathieu *et al.*, 2007) into the *pMDC32* Gateway® vector
345 (pMML058) and the *pGW5* (pKK77). For the reporter constructs, designated *5'TPPJ* regions were
346 *Kpn*I/*Acy*I cloned into the Gateway® *pMDC162* vector to obtain GUS fusions and *5'SPL4* and
347 *5'WUS* regions were *Kpn*I/*Spe*I cloned into *pGREEN800II-LUC* (Hellens *et al*, 2005)(Table S2).
348 *35Somega:LUC-NOS* was used as transformation control in the *5'TPPJ* assays. Protoplasts were
349 isolated from 4-week-old plants, transfected (Wu *et al*, 2009) and incubated for 20h at 22°C and
350 100µmol/$m^{-2}s^{-1}$. Luciferase activity of the *5'TPPJ, 5'SPL4* and *5'WUS* assays was measured with
351 a luciferase and dual-luciferase reporter assay system, respectively (Promega, Madison,
352 Wisconsin, US). GUS activity was determined as described (Yoo *et al*, 2007).

353 EMSA

354 The *WUS* CDS without STOP codon was cloned via the Gateway® entry vector *pDONR207*
355 (pMML059) into a Gateway® destination vector (*pDEST24*). *35S:WUS-GST* (pMML063) was
356 transformed into *Escherichia coli* Rosetta plysS cells and protein production induced with 1mM
357 isopropyl β-D-1-thiogalactopyranoside at 30°C o/n. Cell lysis was performed with 1x sonication of
358 5 sec, 20% power, 4 cycles (Sonoplus Hd 2070 Sonicator, Badelin, Berlin, Germany) in a freshly
359 prepared buffer (20mM Na-phosphate buffer, pH7.4; 0.5MNaCl; 1mM phenylmethylsulfonyl
360 fluoride; 1mM Ethylenediaminetetraacetic acid; 1 tablet cOmplete™ Protease Inhibitor Cocktail
361 (Merck, Darmstadt, Germany) per 10ml buffer). 2µg protein (crude extract, determined by
362 Pierce™ BCA Protein Assay Kit, Thermo Fisher Scientific, Waltham, Massachusetts, US) was
363 used for the EMSA. 50bp, double-stranded, 5′-IRDey-682-labeled probes, spanning the putative
364 $TPPJ^{WUS}$ and WUS^{SPL4} sites are listed in Table S7 (5'*TPPJ*) and Table S8 (5'*WUS*). Binding
365 reactions were carried out with the Odyssey® EMSA Kit (LI-COR®) according to the instructions
366 with a competitor and/or mutated competitor to probe ratio of 1:200 and visualized with the
367 Oddysey Infrafed Imaging System (Li-Cor, Lincoln, NE).

368 Confocal microscopy

369 SAMs of *a TCSn:GFP* cytokinin reporter line (Zurcher *et al.*, 2013) were imaged with a Leica
370 SP8 confocal laser scanning system equipped with a M6000B-CS microscopy stage, an Argon
371 laser (65mV), and a 40x water immersion HCX APO objective as follows: Laser output power
372 20%; GFP excitation (green, wavelength 488nm), emission detection channel 3 (495-520nm),
373 gain PMT 800V; plastid auto-fluorescence (blue), emission detection channel 4 (700-800nm),

374 gain PMT ~500V; scan speed 600Hz in xyz bi-directional scanning mode with a z-stack distance
375 of approx. 10µm. Offset=0; pixel dimension: 1024×1024. Middle sections of representative SAMs
376 were extracted from z-stacks using the Fiji software version 2.0.0-rc-69/1.52 (Schindelin *et al.*,
377 2012).

378 Statistical consideration

379 Statistical significance was analyzed by both one-way ANOVA (Analysis of Variance) with
380 Tukey' Post Hoc HSD (Honestly Significant Difference) based on Tukey-Kramer correction (P
381 value <0.05) or a two-tailed Student's *t*-test.

382 **Acknowledgments**

383 The authors wish to thank all members of the Wahl group for fruitful discussions, M. Schmid and
384 P. Wigge for critical reading of the manuscript, D. Walter for input on statistical analyses, K.
385 Kontbay for providing the SPL4 effector construct, M. Liang and J. Van Dingenen for their support
386 with the *spl* CRISPR/*Cas9* deletion lines, M. Molochko for sharing the *35Somega:LUC-NOS*
387 plasmid, J. Forner for providing the *pJF1031* and *pJF1033* plasmids. Work in the Wahl group was
388 supported by the BMBF (SolaMI, 031B0191), the DFG (SPP1530: WA3639/1-2), and the Max
389 Planck Society.

390 **Author Contributions**

391 VW conceived and designed the experiments and prepared the figures with contributions from
392 MML. VW and MML analyzed the data and wrote the manuscript. MML, KF, AK, and VW
393 performed all essential experiments, i.e. VW generated most of the lines used, except for
394 *ML1:amiRTPPJ* (KF), the *spl* CRISPR/Cas9 deletion lines (MML), and all crosses thereof (MML).
395 MML performed all transactivation assays, ChIP-PCRs, EMSAs and RT-qPCR analyses. MML,
396 AK, KF, CA, and VW analyzed SAM sizes and scored flowering time. RNA *in situ* hybridizations
397 were performed by VW, AK, KF and MML. FK and VW took the confocal images. All authors have
398 read and commented on the text and figures within this manuscript.

399 **Conflict of interest**

400 The authors declare that they don't have any competing commercial interests.

401 **Data Availability Section**

402 Supporting information is provided in a separate file. This includes:

403 Figures S1 to S26

404 Tables S1 to S8

405 SI References

406 **References**

407 Andres F, Coupland G (2012) The genetic basis of flowering responses to seasonal cues. *Nat*
408 *Rev Genet* 13: 627-639

409 Baena-González E, Lunn JE (2020) SnRK1 and trehalose 6-phosphate - two ancient pathways
410 converge to regulate plant metabolism and growth. *Curr Opin Plant Biol* 55: 52-59

411 Baurle I, Laux T (2005) Regulation of WUSCHEL transcription in the stem cell niche of the
412 Arabidopsis shoot meristem. *Plant Cell* 17: 2271-2280

413 Brand U, Fletcher JC, Hobe M, Meyerowitz EM, Simon R (2000) Dependence of stem cell fate in
414 Arabidopsis on a feedback loop regulated by CLV3 activity. *Science (New York, NY)* 289: 617-
415 619

416 Brand U, Grunewald M, Hobe M, Simon R (2002) Regulation of CLV3 expression by two
417 homeobox genes in Arabidopsis. *Plant Physiol* 129: 565-575

418 Busch W, Miotk A, Ariel FD, Zhao Z, Forner J, Daum G, Suzaki T, Schuster C, Schultheiss SJ,
419 Leibfried A *et al* (2010) Transcriptional control of a plant stem cell niche. *Dev Cell* 18: 849-861

420 Caldana C, Martins MCM, Mubeen U, Urrea-Castellanos R (2019) The magic 'hammer' of TOR:
421 the multiple faces of a single pathway in the metabolic regulation of plant growth and
422 development. *Journal of Experimental Botany* 70: 2217-2225

423 Clough SJ, Bent AF (1998) Floral dip: a simplified method for Agrobacterium-mediated
424 transformation of Arabidopsis thaliana. *Plant J* 16: 735-743

425 Czechowski T, Bari RP, Stitt M, Scheible WR, Udvardi MK (2004) Real-time RT-PCR profiling of
426 over 1400 Arabidopsis transcription factors: unprecedented sensitivity reveals novel root- and
427 shoot-specific genes. *Plant J* 38: 366-379

428 Daum G, Medzihradszky A, Suzaki T, Lohmann JU (2014) A mechanistic framework for noncell
429 autonomous stem cell induction in Arabidopsis. *Proc Natl Acad Sci U S A* 111: 14619-14624

430 Fernie AR, Bachem CWB, Helariutta Y, Neuhaus HE, Prat S, Ruan YL, Stitt M, Sweetlove LJ,
431 Tegeder M, Wahl V *et al* (2020) Synchronization of developmental, molecular and metabolic
432 aspects of source-sink interactions. *Nat Plants* 6: 55-66

433 Fichtner F, Lunn JE (2021) The Role of Trehalose 6-Phosphate (Tre6P) in Plant Metabolism and
434 Development. *Annu Rev Plant Biol*

435 Fichtner F, Olas JJ, Feil R, Watanabe M, Krause U, Hoefgen R, Stitt M, Lunn JE (2020)
436 Functional Features of TREHALOSE-6-PHOSPHATE SYNTHASE1, an Essential Enzyme in
437 Arabidopsis. *Plant Cell* 32: 1949-1972

438 Forner J, Pfeiffer A, Langenecker T, Manavella PA, Lohmann JU (2015) Germline-transmitted
439 genome editing in Arabidopsis thaliana Using TAL-effector-nucleases. *PLoS One* 10: e0121056

440 Fouracre JP, Poethig RS (2019) Role for the shoot apical meristem in the specification of juvenile
441 leaf identity in Arabidopsis. *Proc Natl Acad Sci U S A* 116: 10168-10177

442 Gómez LD, Baud S, Gilday A, Li Y, Graham IA (2006) Delayed embryo development in the
443 ARABIDOPSIS TREHALOSE-6-PHOSPHATE SYNTHASE 1 mutant is associated with altered
444 cell wall structure, decreased cell division and starch accumulation. *Plant J* 46: 69-84

445 Graf P, Dolzblasz A, Wurschum T, Lenhard M, Pfreundt U, Laux T (2010) MGOUN1 encodes an
446 Arabidopsis type IB DNA topoisomerase required in stem cell regulation and to maintain
447 developmentally regulated gene silencing. *Plant Cell* 22: 716-728

448 Hellens RP, Allan AC, Friel EN, Bolitho K, Grafton K, Templeton MD, Karunairetnam S, Gleave
449 AP, Laing WA (2005) Transient expression vectors for functional genomics, quantification of
450 promoter activity and RNA silencing in plants. *Plant Methods* 1: 13

451 Hyun Y, Richter R, Coupland G (2017) Competence to Flower: Age-Controlled Sensitivity to
452 Environmental Cues. *Plant Physiol* 173: 36-46

453 Hyun Y, Richter R, Vincent C, Martinez-Gallegos R, Porri A, Coupland G (2016) Multi-layered
454 Regulation of SPL15 and Cooperation with SOC1 Integrate Endogenous Flowering Pathways at
455 the Arabidopsis Shoot Meristem. *Dev Cell* 37: 254-266

456 Jacqmard A, Gadisseur I, Bernier G (2003) Cell division and morphological changes in the shoot
457 apex of Arabidopsis thaliana during floral transition. *Ann Bot* 91: 571-576

458 Jung JH, Lee HJ, Ryu JY, Park CM (2016) SPL3/4/5 Integrate Developmental Aging and
459 Photoperiodic Signals into the FT-FD Module in Arabidopsis Flowering. *Mol Plant* 9: 1647-1659

460 Kaufmann K, Muino JM, Osteras M, Farinelli L, Krajewski P, Angenent GC (2010) Chromatin
461 immunoprecipitation (ChIP) of plant transcription factors followed by sequencing (ChIP-SEQ) or
462 hybridization to whole genome arrays (ChIP-CHIP). *Nat Protoc* 5: 457-472

463 Kinoshita A, Vayssieres A, Richter R, Sang Q, Roggen A, van Driel AD, Smith RS, Coupland G
464 (2020) Regulation of shoot meristem shape by photoperiodic signaling and phytohormones during
465 floral induction of Arabidopsis. *Elife* 9

466 Klepikova AV, Logacheva MD, Dmitriev SE, Penin AA (2015) RNA-seq analysis of an apical
467 meristem time series reveals a critical point in Arabidopsis thaliana flower initiation. *BMC*
468 *Genomics* 16: 466

469 Kwiatkowska D (2008) Flowering and apical meristem growth dynamics. *J Exp Bot* 59: 187-201

470 Leibfried A, To JP, Busch W, Stehling S, Kehle A, Demar M, Kieber JJ, Lohmann JU (2005)
471 WUSCHEL controls meristem function by direct regulation of cytokinin-inducible response
472 regulators. *Nature* 438: 1172-1175

473 Lin TF, Saiga S, Abe M, Laux T (2016) OBE3 and WUS Interaction in Shoot Meristem Stem Cell
474 Regulation. *PLoS One* 11: e0155657

475 Lohmann JU, Hong RL, Hobe M, Busch MA, Parcy F, Simon R, Weigel D (2001) A molecular link
476 between stem cell regulation and floral patterning in Arabidopsis. *Cell* 105: 793-803

477 Mathieu J, Warthmann N, Kuttner F, Schmid M (2007) Export of FT protein from phloem
478 companion cells is sufficient for floral induction in Arabidopsis. *Curr Biol* 17: 1055-1060

479 McElver J, Tzafrir I, Aux G, Rogers R, Ashby C, Smith K, Thomas C, Schetter A, Zhou Q,
480 Cushman MA *et al* (2001) Insertional mutagenesis of genes required for seed development in
481 Arabidopsis thaliana. *Genetics* 159: 1751-1763

482 Olas JJ, Van Dingenen J, Abel C, Dzialo MA, Feil R, Krapp A, Schlereth A, Wahl V (2019) Nitrate
483 acts at the Arabidopsis thaliana shoot apical meristem to regulate flowering time. *New Phytol* 223:
484 814-827

485 Pfeiffer A, Janocha D, Dong Y, Medzihradszky A, Schone S, Daum G, Suzaki T, Forner J,
486 Langenecker T, Rempel E *et al* (2016) Integration of light and metabolic signals for stem cell
487 activation at the shoot apical meristem. *Elife* 5

488 Pfeiffer A, Wenzl C, Lohmann JU (2017) Beyond flexibility: controlling stem cells in an ever
489 changing environment. *Curr Opin Plant Biol* 35: 117-123

490 Ponnu J, Schlereth A, Zacharaki V, Dzialo MA, Abel C, Feil R, Schmid M, Wahl V (2020) The
491 Trehalose 6-Phosphate Pathway Impacts Vegetative Phase Change in Arabidopsis thaliana.
492 *Plant J*

493 Ruf S, Forner J, Hasse C, Kroop X, Seeger S, Schollbach L, Schadach A, Bock R (2019) High-
494 efficiency generation of fertile transplastomic Arabidopsis plants. *Nat Plants* 5: 282-289

495 Schindelin J, Arganda-Carreras I, Frise E, Kaynig V, Longair M, Pietzsch T, Preibisch S, Rueden
496 C, Saalfeld S, Schmid B *et al* (2012) Fiji: an open-source platform for biological-image analysis.
497 *Nat Methods* 9: 676-682

498 Schmid M, Uhlenhaut NH, Godard F, Demar M, Bressan R, Weigel D, Lohmann JU (2003)
499 Dissection of floral induction pathways using global expression analysis. *Development* 130: 6001-
500 6012

501 Schwab R, Ossowski S, Riester M, Warthmann N, Weigel D (2006) Highly specific gene silencing
502 by artificial microRNAs in Arabidopsis. *Plant Cell* 18: 1121-1133

503 Sloan J, Hakenjos JP, Gebert M, Ermakova O, Gumiero A, Stier G, Wild K, Sinning I, Lohmann
504 JU (2020) Structural basis for the complex DNA binding behavior of the plant stem cell regulator
505 WUSCHEL. *Nat Commun* 11

506 Snipes SA, Rodriguez K, DeVries AE, Miyawaki KN, Perales M, Xie M, Reddy GV (2018)
507 Cytokinin stabilizes WUSCHEL by acting on the protein domains required for nuclear enrichment
508 and transcription. *PLoS Genet* 14: e1007351

509 Sonoda Y, Yao SG, Sako K, Sato T, Kato W, Ohto MA, Ichikawa T, Matsui M, Yamaguchi J,
510 Ikeda A (2007) SHA1, a novel RING finger protein, functions in shoot apical meristem
511 maintenance in Arabidopsis. *Plant J* 50: 586-596

512 Srikanth A, Schmid M (2011) Regulation of flowering time: all roads lead to Rome. *Cellular and*
513 *molecular life sciences : CMLS* 68: 2013-2037

514 Torti S, Fornara F, Vincent C, Andres F, Nordstrom K, Gobel U, Knoll D, Schoof H, Coupland G
515 (2012) Analysis of the Arabidopsis shoot meristem transcriptome during floral transition identifies
516 distinct regulatory patterns and a leucine-rich repeat protein that promotes flowering. *The Plant*
517 *cell* 24: 444-462

518 Varkonyi-Gasic E, Wu R, Wood M, Walton EF, Hellens RP (2007) Protocol: a highly sensitive RT-
519 PCR method for detection and quantification of microRNAs. *Plant Methods* 3: 12

520 Wahl V, Ponnu J, Schlereth A, Arrivault S, Langenecker T, Franke A, Feil R, Lunn JE, Stitt M,
521 Schmid M (2013) Regulation of flowering by trehalose-6-phosphate signaling in Arabidopsis
522 thaliana. *Science (New York, NY)* 339: 704-707

523 Wang JW, Czech B, Weigel D (2009) miR156-regulated SPL transcription factors define an
524 endogenous flowering pathway in Arabidopsis thaliana. *Cell* 138: 738-749

525 Wang ZP, Xing HL, Dong L, Zhang HY, Han CY, Wang XC, Chen QJ (2015) Egg cell-specific
526 promoter-controlled CRISPR/Cas9 efficiently generates homozygous mutants for multiple target
527 genes in Arabidopsis in a single generation. *Genome Biol* 16: 144

528 Wisman E, Cardon GH, Fransz P, Saedler H (1998) The behaviour of the autonomous maize
529 transposable element En/Spm in Arabidopsis thaliana allows efficient mutagenesis. *Plant Mol Biol*
530 37: 989-999

531 Wu FH, Shen SC, Lee LY, Lee SH, Chan MT, Lin CS (2009) Tape-Arabidopsis Sandwich - a
532 simpler Arabidopsis protoplast isolation method. *Plant Methods* 5: 16

533 Wu G, Poethig RS (2006) Temporal regulation of shoot development in Arabidopsis thaliana by
534 miR156 and its target SPL3. *Development (Cambridge, England)* 133: 3539-3547

535 Xie Y, Zhou Q, Zhao Y, Li Q, Liu Y, Ma M, Wang B, Shen R, Zheng Z, Wang H (2020) FHY3 and
536 FAR1 Integrate Light Signals with the miR156-SPL Module-Mediated Aging Pathway to Regulate
537 Arabidopsis Flowering. *Mol Plant* 13: 483-498

538 Xu M, Hu T, Zhao J, Park MY, Earley KW, Wu G, Yang L, Poethig RS (2016) Developmental
539 Functions of miR156-Regulated SQUAMOSA PROMOTER BINDING PROTEIN-LIKE (SPL)
540 Genes in Arabidopsis thaliana. *PLoS Genet* 12: e1006263

541 Yadav RK, Perales M, Gruel J, Girke T, Jonsson H, Reddy GV (2011) WUSCHEL protein
542 movement mediates stem cell homeostasis in the Arabidopsis shoot apex. *Genes Dev* 25: 2025-
543 2030

544 Yamaguchi N, Winter CM, Wu MF, Kanno Y, Yamaguchi A, Seo M, Wagner D (2014) Gibberellin
545 acts positively then negatively to control onset of flower formation in Arabidopsis. *Science (New*
546 *York, NY)* 344: 638-641

547 Yang L, Xu M, Koo Y, He J, Poethig RS (2013) Sugar promotes vegetative phase change in
548 Arabidopsis thaliana by repressing the expression of MIR156A and MIR156C. *Elife* 2: e00260

549 Yoo SD, Cho YH, Sheen J (2007) Arabidopsis mesophyll protoplasts: a versatile cell system for
550 transient gene expression analysis. *Nat Protoc* 2: 1565-1572

551 Yu S, Cao L, Zhou CM, Zhang TQ, Lian H, Sun Y, Wu J, Huang J, Wang G, Wang JW (2013)
552 Sugar is an endogenous cue for juvenile-to-adult phase transition in plants. *Elife* 2: e00269

553 Zurcher E, Tavor-Deslex D, Lituiev D, Enkerli K, Tarr PT, Muller B (2013) A robust and sensitive
554 synthetic sensor to monitor the transcriptional output of the cytokinin signaling network in planta.
555 *Plant Physiol* 161: 1066-1075

556

All main figures for

Sugar Signaling Induces Dynamic Changes During Meristem Development to Regulate Flowering in Arabidopsis

Magdalena Musialak-Lange[1], Katharina Fiddeke[1,#], Annika Franke[1,#], Friedrich Kragler[1], Christin Abel[1], and Vanessa Wahl[1,*]

Affiliations: [1]Max Planck Institute of Molecular Plant Physiology, Department of Metabolic Networks, Am Mühlenberg 1, Potsdam, 14476, Germany.

[#]K.F. and A.F. contributed equally

[*]**Correspondence**: Vanessa Wahl

Email: vanessa.wahl@mpimp-golm.mpg.de

Synopsis:

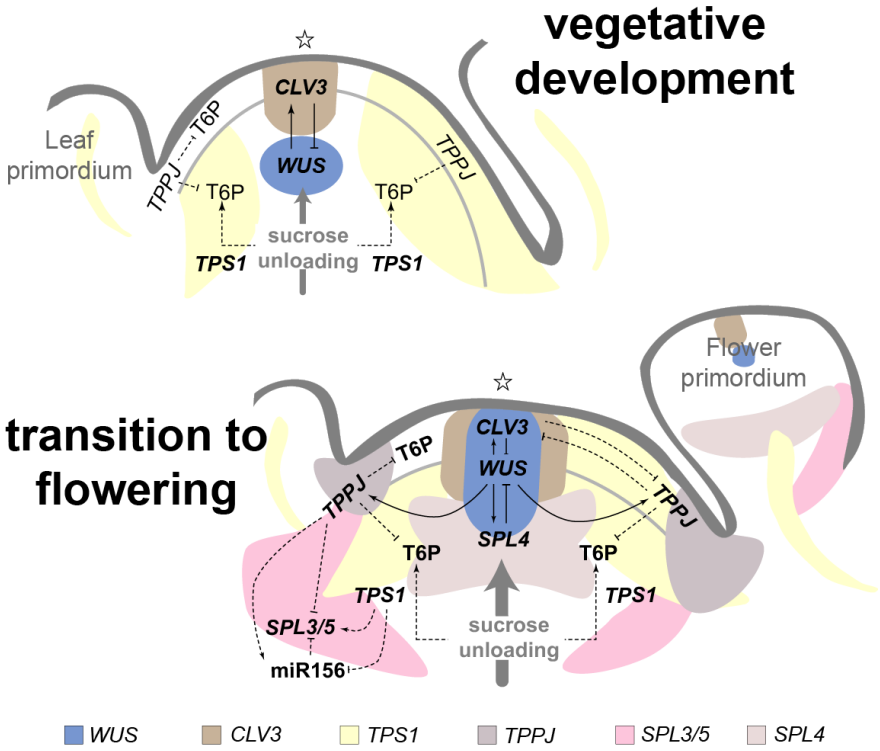

Schematic illustration of dynamic feedback-regulations between sugar signaling, meristem maintenance and the age pathway of the flowering network in the transition SAM as compared to the vegetative SAM.
During vegetative growth SAM maintenance is controlled by spatially separated *WUS* and *CLV3* expression in a negative feedback-loop. At floral transition increased activity of the T6P pathway in the SAM uncouples this regulation. This results in an unreported special relocation of *WUS* expression and involves a transient negative feedback-loop between WUS and SPL4.

Figures

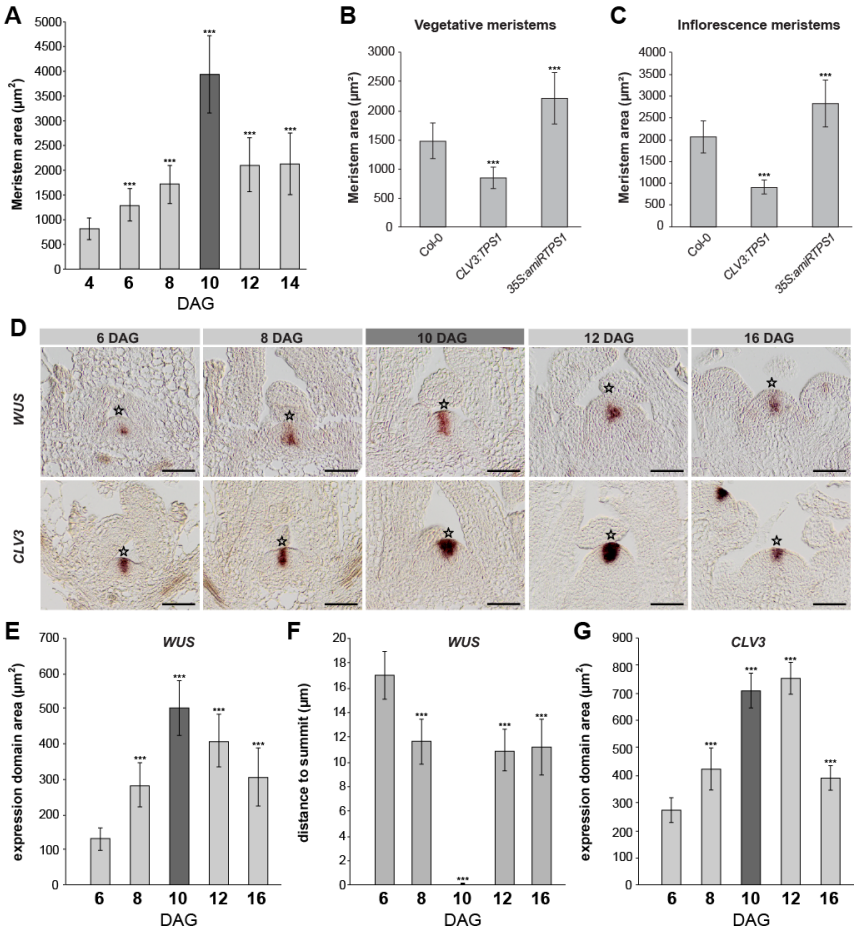

Figure 1. The T6P pathway impacts SAM size during development. (*A*) SAM area throughout development. n=15 (*B*) Vegetative and (*C*) inflorescence SAM size of *CLV3:TPS1* and *35S:amiRTPS1* lines. n=10. (*D*) *WUS* and *CLV3* expression by RNA *in situ* hybridization in vegetative (6 and 8 DAG), transition (10 DAG, marked dark grey) and inflorescence SAMs (12 and 16 DAG) of LD-grown Col-0 plants. (*E*) *WUS* expression domain sizes, (*F*) *WUS* expression domain distance to SAM summit, and (*G*) *CLV3* expression domain area, in vegetative, transition (dark grey) and inflorescence SAMs of LD-grown wild-type plants. n>10. Error bars denote s.d.; significance was calculated based on a Student's *t*-test, ***P<0.001. Star indicates SAM summit. Scale bars 25µm.

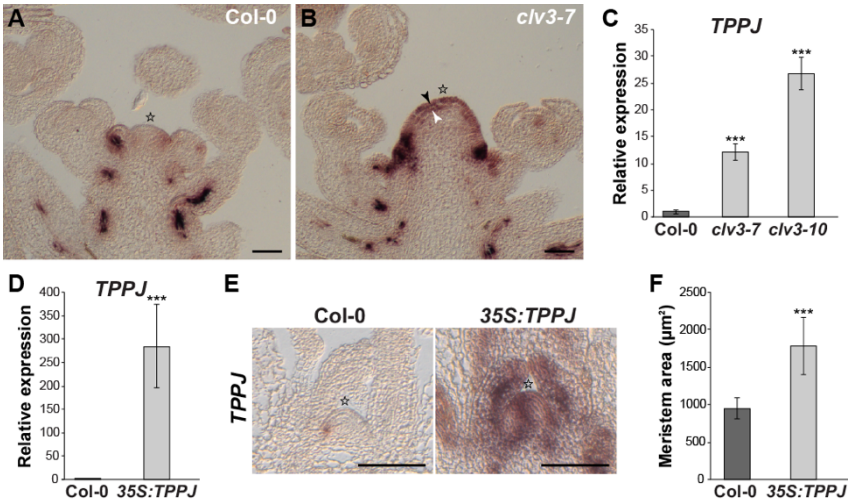

Figure 2. *WUS* and *CLV3* expression in response to changes of *TPPJ* in the SAM. (*A*, *B*) *TPPJ* expression by RNA *in situ* hybridization on longitudinal sections through inflorescence SAMs of (*A*) Col-0, and (*B*) *clv3-7*, and by RT-qPCR in apices collected from (*C*) *clv3-7*, *clv3-10*, and (*D*) *35S:TPPJ* plants. n=3. (*E*) Expression of *TPPJ* by RNA *in situ* hybridization on longitudinal sections through inflorescence SAMs of Col-0 and *35S:TPPJ.* (*F*) SAM size of plants overexpressing *TPPJ*. n=10. Error bars denote s.d.; significance calculated by one-way ANOVA (C,D) and Student's *t*-test (F), ***P<0.001. Stars indicates SAM summit. Scale bars are 50µm.

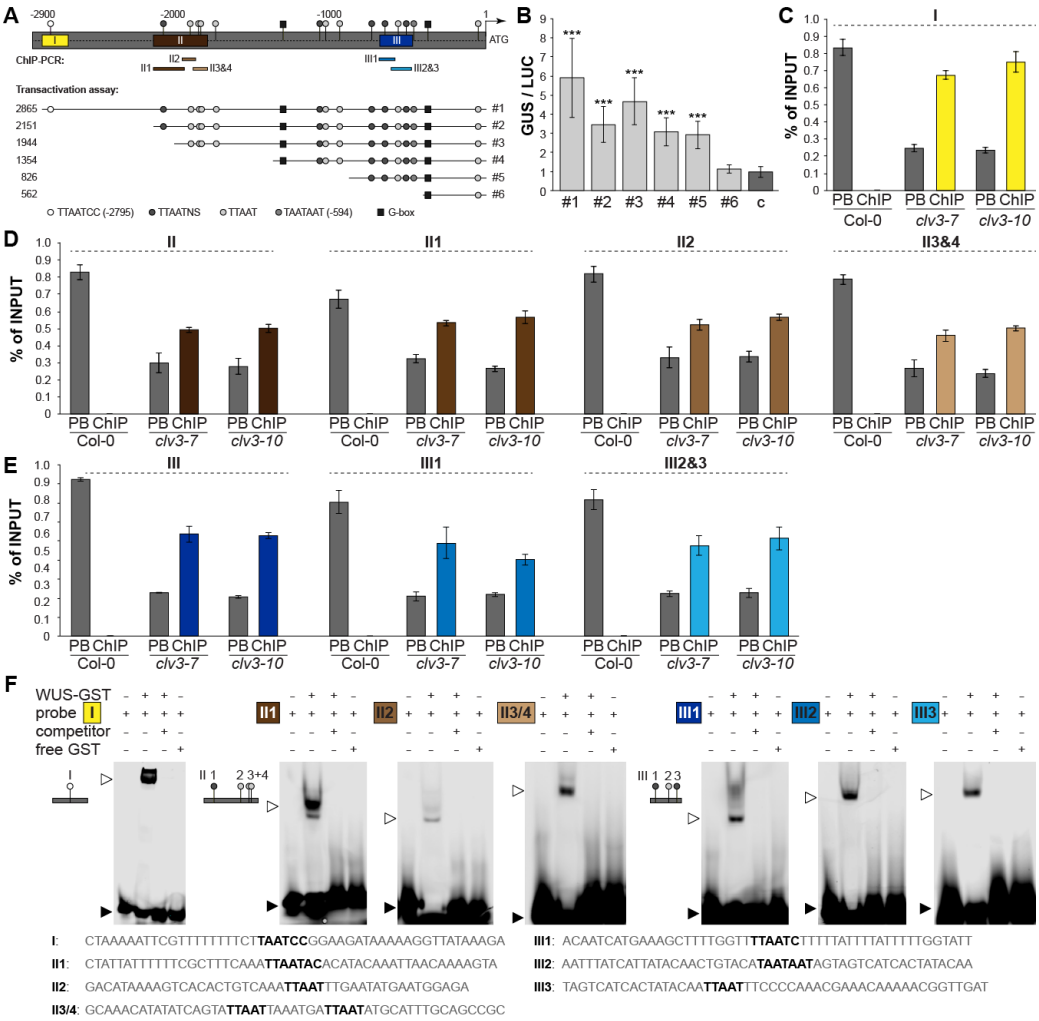

Figure 3. WUS directly regulates *TPPJ* in the SAM. (*A*) Overview of *TPPJ* 5' regulatory region with putative *TPPJ*^{WUS} sites (grey circles, black boxes), position of ChIP-PCR amplicons corresponding to the results shown in (C-E). Boxes marked with I, II, and III indicate *5' TPPJ* regions with in total seven confirmed core *TPPJ*^{WUS} sites – I: -2795 – -2789 bp, II: -2073 – -1830 bp, and III: -652 – -564 bp. Sequence location and lengths used in (B) indicated with #1-6. (*B*) Protoplast transactivation assay showing activation of the GUS reporter when coupled to the regions indicated in (A), relative to LUC activity. c indicates untransformed control. n=6. (*C-E*) Enrichment of (*C*) region I, (*D*) region II, and (*E*) region III as indicated in (A) measured by ChIP-PCR relative to the input. PB – post binding fraction. n=3. (*F*) EMSA for WUS binding to the indicated regions (A, I-III). Shifted band in the presence of WUS protein (open arrow head), non-shifted fraction (closed arrow head). Error bars denote s.d.; significance based on one-way ANOVA, ***P<0.001. Scale bars are 50µm.

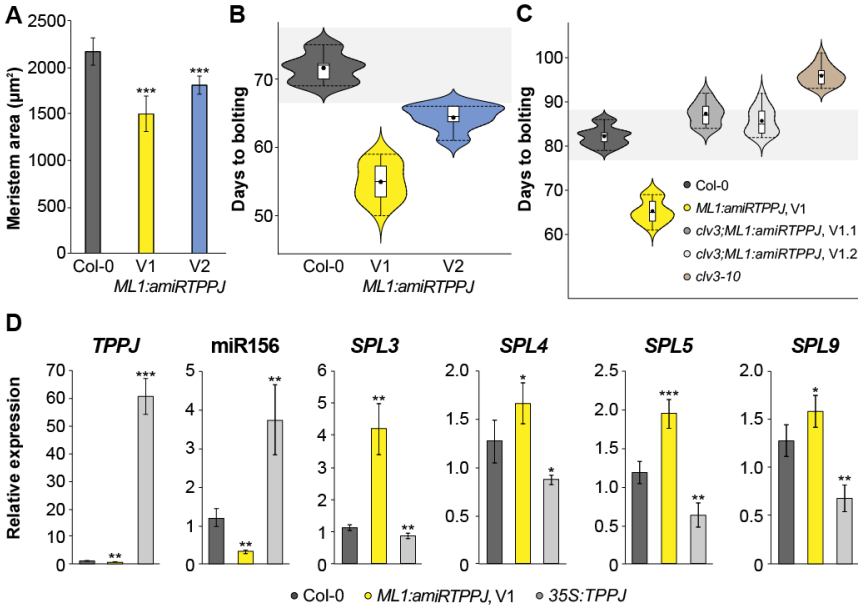

Figure 4. The role of TPPJ in the outer SAM layer. (*A*) Meristem area of Col-0, *ML1:amiRTPPJ* V1 and V2. n=10. (*B*,*C*) Flowering time of (*B*) *ML1:amiRTPPJ* and (*C*) *clv3-10;ML1:amiRTPPJ* shown as days to bolting, relative to the wild type. V1 and V2 indicate two independent versions of artificial microRNAs designed to target *TPPJ* transcript. n=22. (*D*) Relative expression of *SPL* genes in SD-grown *ML1:amiRTPPJ* and *35S:TPPJ* at 40 days after germination. n=4. Error bars denote s.d.; significance calculated based on one-way ANOVA (D) and Student's *t*-test (A); **P*<0.05, ***P*<0.01, ****P*<0.001.

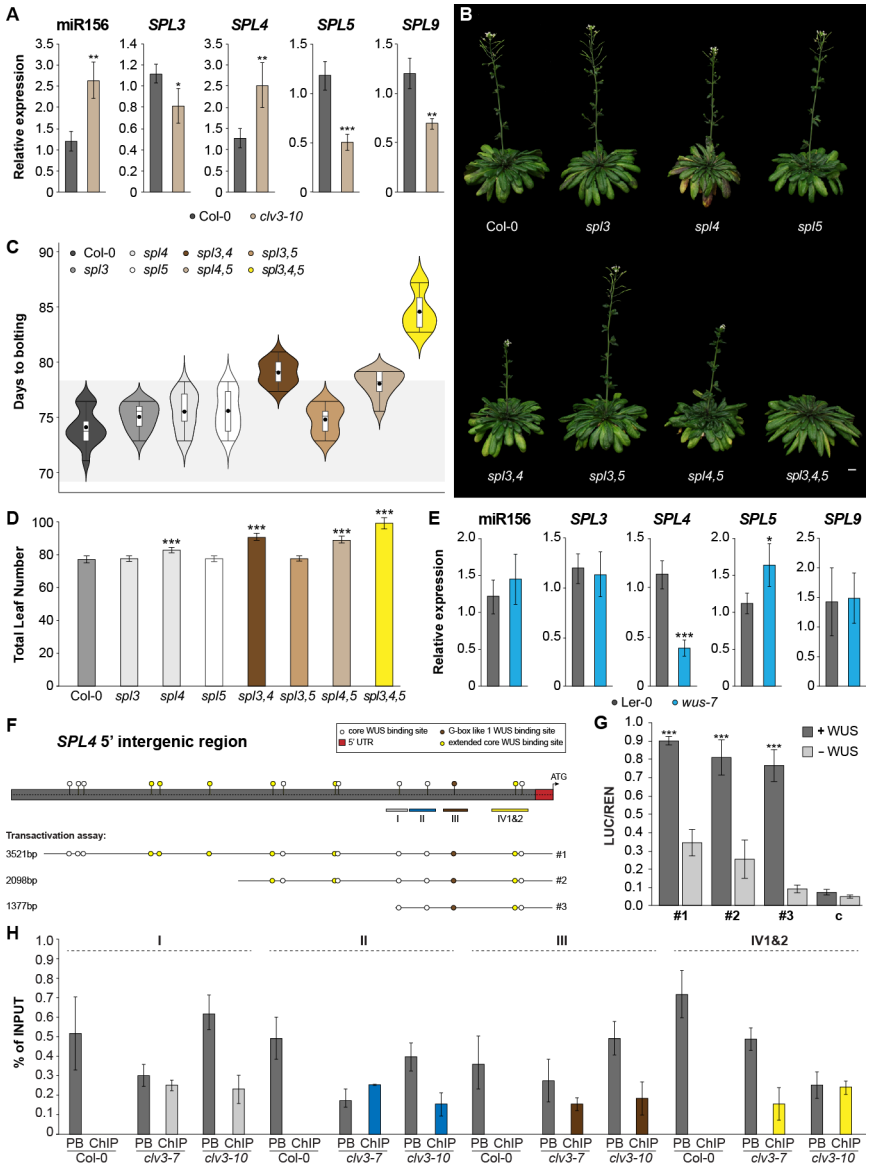

Figure 5. WUS activates *SPL4*. (*A*) Relative expression of mature miRNA and *SPL* genes in SD-grown Col-0 and *clv3-10* apices. n=4 (*B*) Representative pictures of *SPL3-5* single, double and triple CRISPR/*Cas9* deletion mutants in comparison to Col-0 grown in SD. (*C*) Flowering time of deletion mutants displayed in (B) provided as days to bolting and (*D*) total leaf numbers. n=25. (*E*) Relative expression of mature miRNA and *SPL* genes in SD-grown Ler-0 and *wus-7* apices (*F*) Overview of *SPL4* 5' regulatory region with putative $SPL4^{WUS}$ sites (grey, yellow and white circles) and position of ChIP-PCR amplicons (grey, blue and yellow boxes) corresponding to the results shown in (G, H). Boxes marked with I, II, III and IV (1&2) indicate *5' SPL4* regions with in total five core $SPL4^{WUS}$ sites – I: -1073 – -1068 bp, II: -880 – -875 bp, III: -697 – -691, IV1: -259 – -252 and IV2: -214 – -209 bp. Sequence location and lengths used in (G) indicated with #1-3. (*G*) Protoplast transactivation assay showing activation of the reporter (LUC) when coupled to the regions indicated in (F), relative to REN activity. c indicates vector control. n=3. (*H*) Enrichment of regions I, II, III and IV1&2 as indicated in (F) measured by ChIP-PCR relative to the input in *clv3-7* and *clv3-10* apices. PB – post binding fraction. n=3. Error bars denote s.d.; significance calculated based on one-way ANOVA (A, G) and Student's *t*-test (D); *P<0.05, ***P*<0.01, ****P*<0.001.

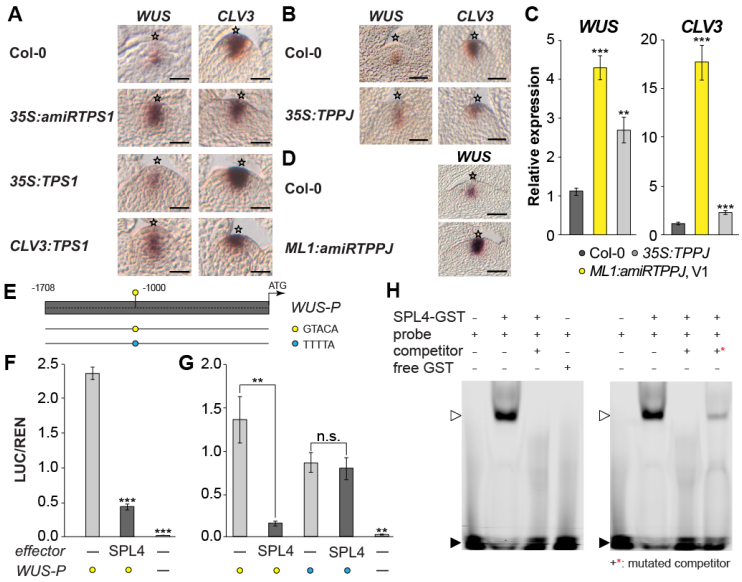

Figure 6. SPL4 negatively feeds back to *WUS.* (*A*,*B*) *WUS* and *CLV3* expression by RNA *in situ* hybridization on (*A*) longitudinal sections through Col-0, *35S:amiRTPS1, 35S:TPS1* and *CLV3:TPS1* and (*B*) Col-0, and *35S:TPPJ* apices of LD-grown plants. (*C*) Relative expression of *WUS* and *CLV3* in SD-grown Col-0, *35S:TPPJ* and *ML1:amiRTPPJ* V1 apices. n=4 (*D*) RNA *in situ* hybridization on longitudinal sections through Col-0, and *35S:amiRTPPJ* apices. n=3. (*E*) Overview of *WUS* 5' regulatory region with putative WUS^{SPL} site corresponding to the results shown in (F,G,H). Grey box indicates *5' WUS* region with the native and mutated core WUS^{SPL} site -1067 – -1063 bp (yellow and blue circles, respectively). Sequence location and lengths used in (F,G) indicated as lines below. (*F,G*) Protoplast transactivation assay showing repression of the reporter (LUC) when coupled to the *5'WUS* region indicated in (E), (*F*) relative to REN activity of the native *5'WUS*, and (*G*) the comparison of the native and the mutated WUS^{SPL} site (yellow and blue circles, respectively), n=3. (*H*) EMSA for SPL4 binding to the WUS^{SPL} site (E). Shifted band in the presence of SPL4 protein (open arrow head), non-shifted fraction (closed arrow head). Please note the shift in the presence of the mutated competitor (+*), indicating specificity of binding. Error bars denote s.d.; significance calculated based on one-way ANOVA; $^{**}P<0.01$, $^{***}P<0.001$. Scale bars: 25µm. Star indicates SAM summit.

Supplementary Information for

Sugar Signaling Induces Dynamic Changes During Meristem Development to Regulate Flowering in Arabidopsis

Magdalena Musialak-Lange[1], Katharina Fiddeke[1,#], Annika Franke[1,#], Friedrich Kragler[1], Christin Abel[1], and Vanessa Wahl[1,*]

Affiliations: [1]Max Planck Institute of Molecular Plant Physiology, Department of Metabolic Networks, Am Mühlenberg 1, Potsdam, 14476, Germany. [#]K.F. and A.F. contributed equally

[*]**Correspondence**: Vanessa Wahl

Email: vanessa.wahl@mpimp-golm.mpg.de

This PDF file includes:

Figures S1 to S25
Tables S1 to S8
SI References

Supplementary Information

Supplementary Figures

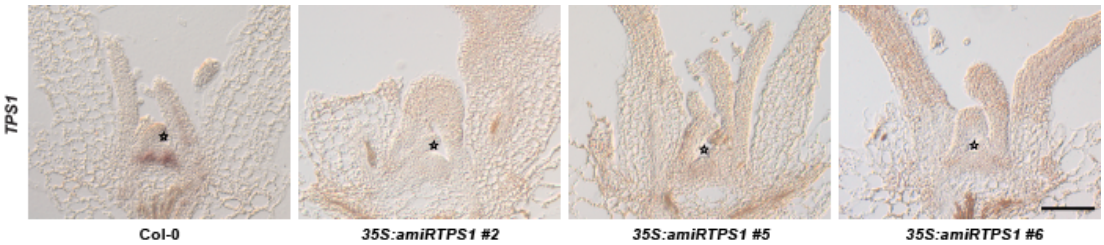

Fig. S1. *TPS1* expression at the shoot apical meristem of *35S:amiRTPS1* plants. Downregulation of *TPS1* by overexpressing an artificial microRNA targeting *TPS1* (*35S:amiRTPS1*) in plants of three independent lines (#2, #5 and #6; (Wahl *et al*, 2013)) as analyzed by RNA *in situ* hybridization using a specific probe against *TPS1*. Pictures depict representative longitudinal middle sections through vegetative apices (8 DAG in LD) of Col-0 and *35S:amiRTPS1*, respectively. Line #6 was used for the experiments in this study. Star indicates SAM summit. Scale bar is 50 µm**.**

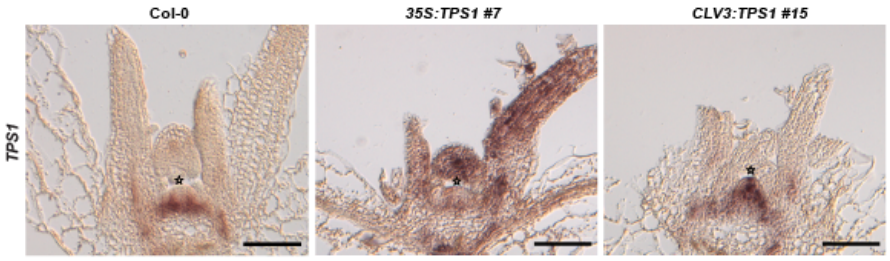

Fig. S2. *TPS1* expression at the shoot apical meristem of *35S:TPS1* and *CLV3:TPS1* plants. In comparison to expression in Col-0 *TPS1* was generally found upregulated in plants overexpressing *TPS1* (*35S:TPS1*, #7) and the central zone when expressing it under the control of the *CLAVATA3* (*CLV3*) promoter (*CLV3:TPS1*, #15) as analyzed by RNA *in situ* hybridization using a specific probe against *TPS1*. Pictures depict representative longitudinal middle sections through vegetative apices (8 DAG in LD) of Col-0, *35S:TPS1*, and *CLV3:TPS1*, respectively. Star indicates SAM summit. Scale bars are 50 µm.

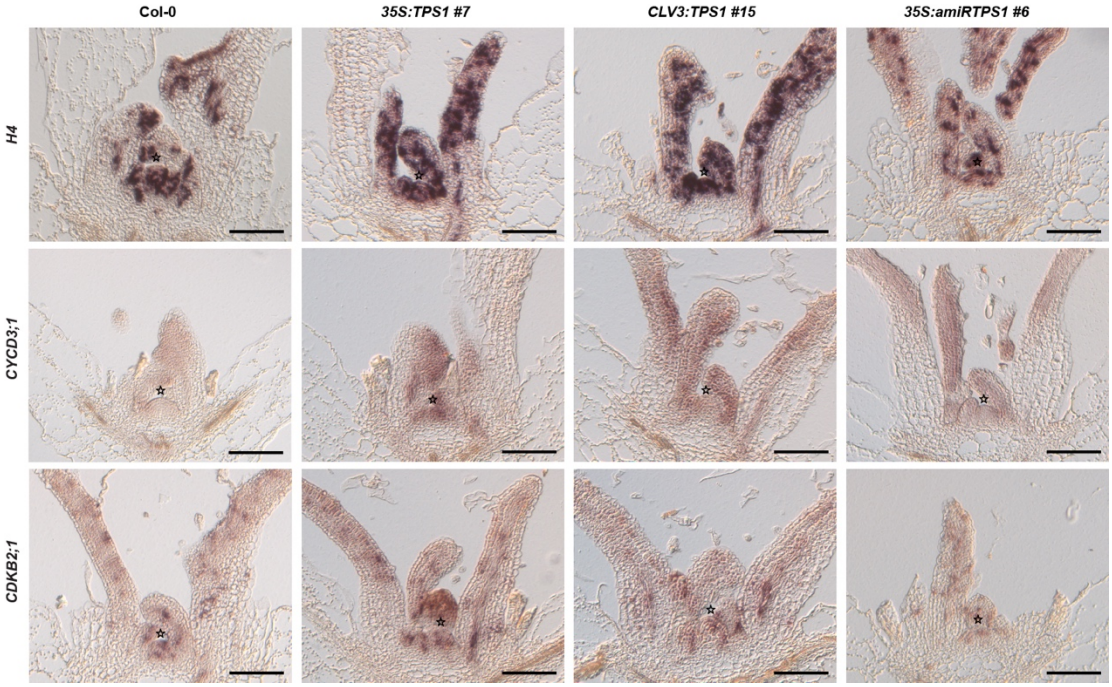

Fig. S3. Cell cycle gene expression at the shoot apical meristem of *35S:TPS1, CLV3:TPS1* and *35S:amiRTPS1* plants. RNA *in situ* hybridization using specific probes for *HISTONE H4* (*H4*), *CYCLIN D3;1* (*CYCD3;1*) and *CYCLIN-DEPENDENT KINASE 2;1* (*CDKB2;1*) to illustrate expression in longitudinal middle sections through the SAM of Col-0, *35S:TPS1* (#7), *CLV3:TPS1* (#15) and *35S:amiRTPS1* (#6). Star indicates SAM summit. Scale bars are 50 µm.

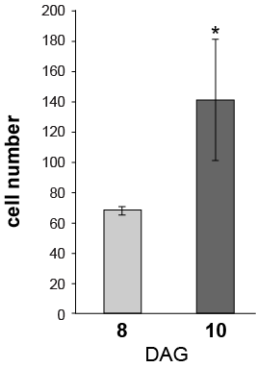

Fig. S4. Metrics at the SAM before and at the floral transition. Cell numbers as recorded at 8 (vegetative SAM) and 10 days (transition SAM) after germination (DAG). Significance calculated based on one-way Anova; *P<0.05.

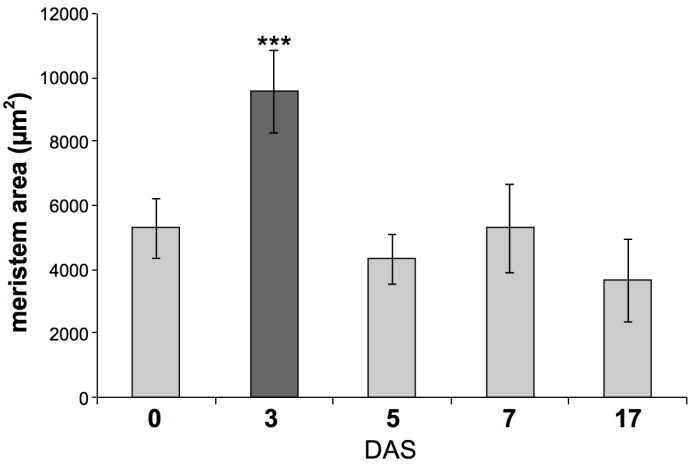

Fig. S5. Shoot apical meristem area of SD-grown and LD-induced plants. Vegetative and inflorescence SAM areas (light grey), and transition SAM area (dark grey) of wild-type plants grown in SD for 30 days and transferred to LD for 3, 5, 7 and 17 days (DAS). Error bars denote s.d.; ***P<0.001 in relation to 0 days after transfer to LD (Student's t-test).

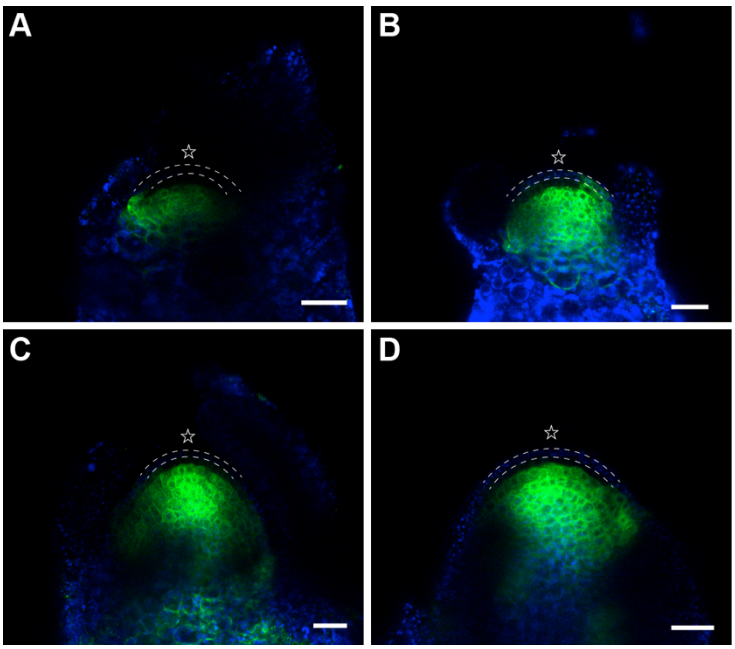

Fig. S6. Analysis of the cytokinin signaling reporter TCSn:GFP. Representative confocal laser scanning microscope images of SAMs of (*A*) 6 DAG, (*B*) 8 DAG, (*C*) 10 DAG, and (*D*) 12 DAG of TCSn:GFP cytokinin reporter line (green (Zurcher *et al*, 2013); blue – autofluorescence of chloroplasts). Please note the absence of cytokinin signal in the L1 (between dashed lines) and L2 (cell layers below) in the meristem proper. Star indicates SAM summit, scale bars are 25μm.

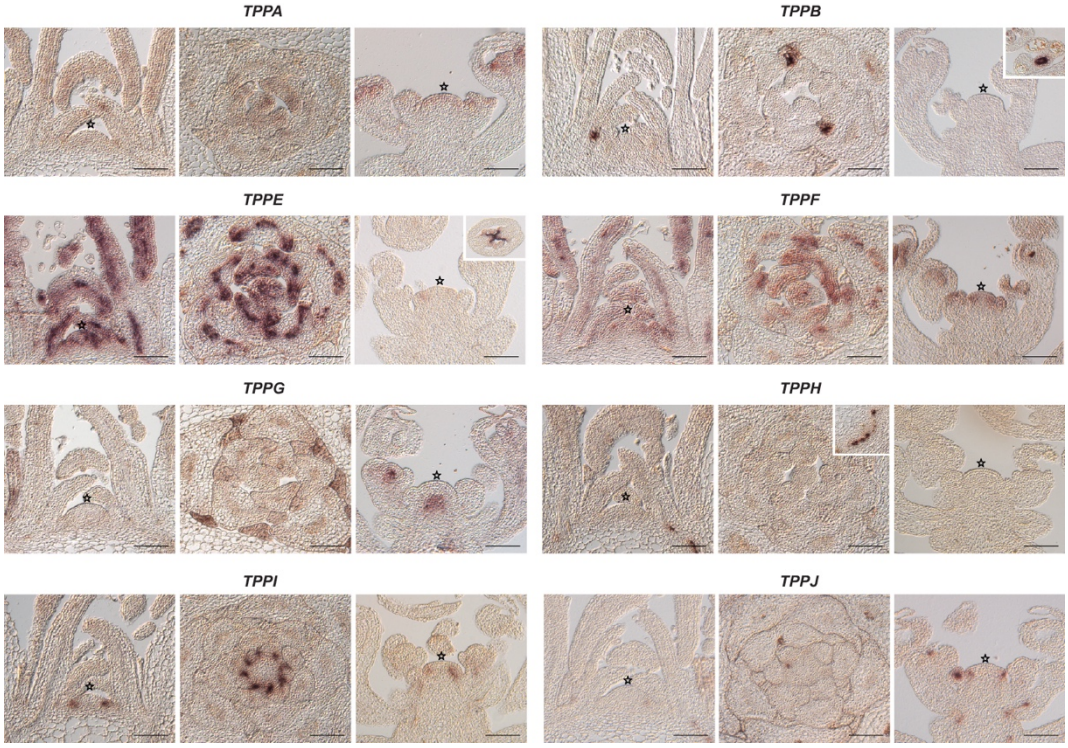

Fig. S7. Expression of Arabidopsis *TPP* genes at the shoot apical meristem detected by RNA *in situ* hybridization. The individual panels contain: a longitudinal middle section and a cross section through a vegetative Col-0 apex and a longitudinal middle section through an inflorescence apex. Representative pictures of *TPPC* and *TPPD* were omitted from this figure, since their specific probes gave no signal, indicating that transcripts of *TPPC* and *TPPD* were below detection limit in the tissues and/or stages analyzed. Star indicates SAM summit. Scale bars are 100 μm.

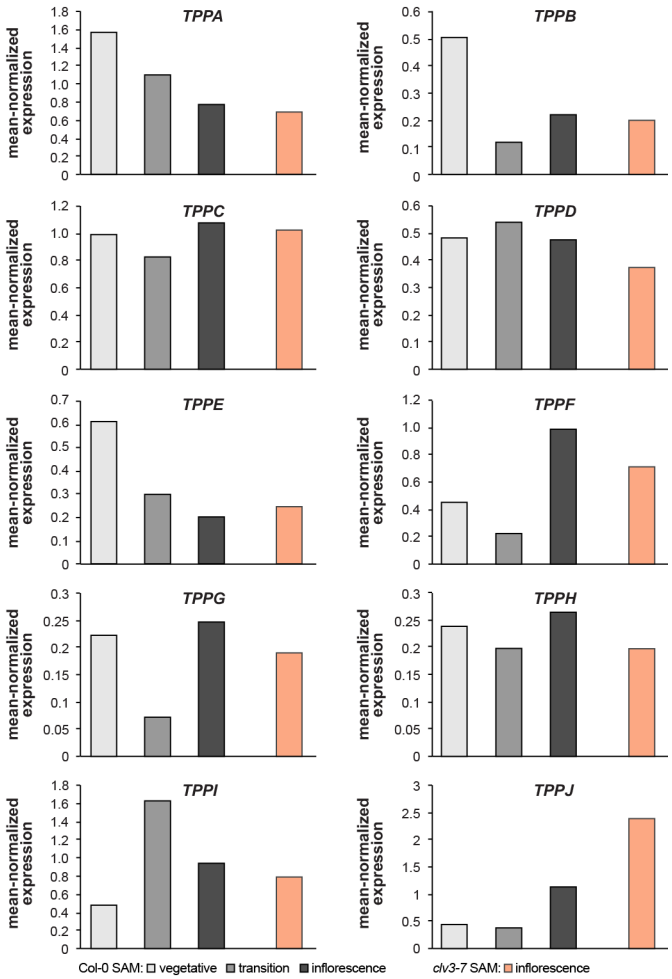

Fig. S8. AtGenExpress expression profiles of the Arabidopsis *TPP* genes. Values for Col-0 vegetative, transition and inflorescence apices (grey scale) and *clv3-7* inflorescence apices (orange) extracted from data deposited for (Schmid *et al*, 2005). All data points were mean-normalized.

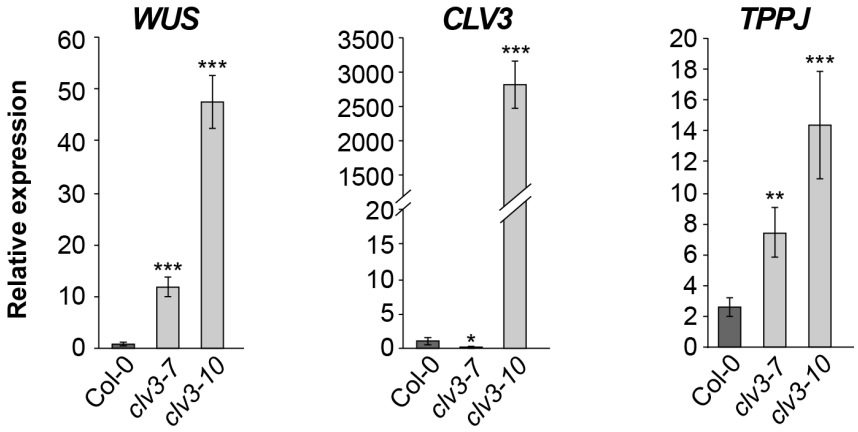

Fig. S9. Expression of meristem maintenance genes and *TPPJ* in the *clv3-7* and *clv3-10* mutant SAM. RT-qPCR results of *TPPJ*, *WUS* and *CLV3* expression in SD-grown *clv3-7* and *clv3-10* SAMs, harvested 40 days after germination. Please note that the graph for *TPPJ* is a biological repetition of the graph in Figure 2C. Please also note that *clv3-10* is a TALEN generated mutant with a five nucleotide deletion in the last exon, which renders the transcript inactive to produce a functional protein (Forner *et al*, 2015). This is the cause for increased expression of *CLV3* downstream of increased *WUS* in the *clv3-10* mutant background. Error bars denote s.d.; *P<0.05, **P<0.01, ***P<0.001 (one-way ANOVA).

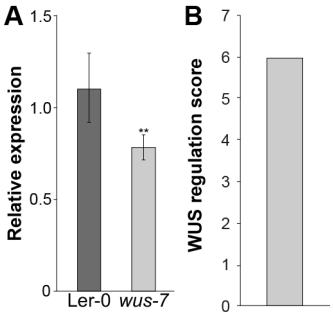

Fig. S10. *TPPJ* Expression in *WUS* transgenic lines. *(A)* RT-qPCR results of *TPPJ* expression in SD-grown *wus-7* as compared to wild-type Ler-0 SAMs, harvested 30 days after germination. Error bars denote s.d.; **P<0.01, (one-way ANOVA). (*B*) *TPPJ* expression is increased upon WUS induction as shown by a WUS regulation score (WRS). According to Busch and colleagues, the WRS quantifies gene expression in response to a modulation in WUS activity normalized to the average response of all genes. Values extracted form a data set, deposited as a supplemental material of a publication by (Busch *et al*, 2010).

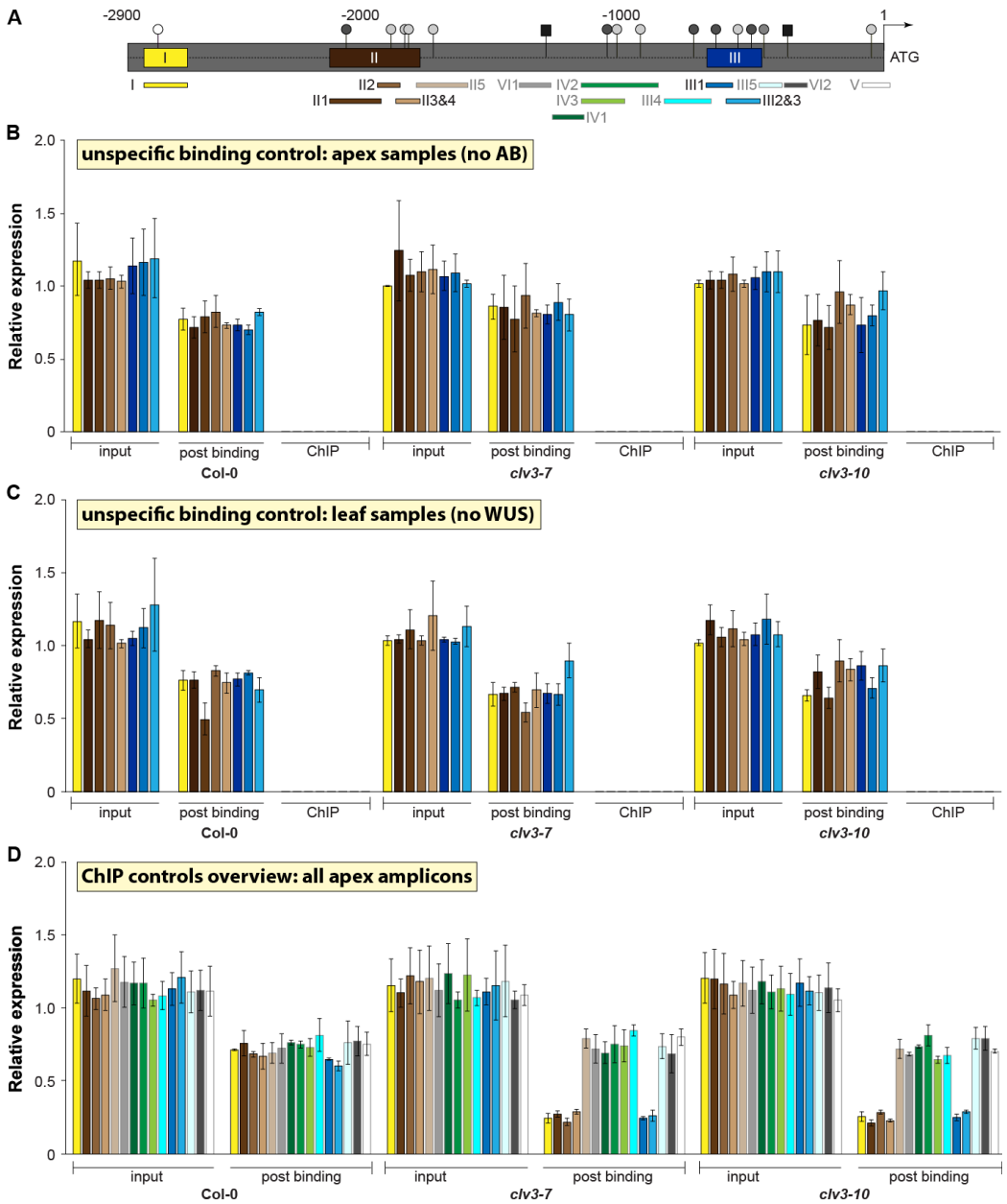

Fig. S11. ChIP-PCR control experiments for Figure 3C-E. (*A*) Overview of *5'TPPJ* intergenic sequence with all investigated putative $TPPJ^{WUS}$ sites (grey circles, black boxes), position of ChIP-PCR amplicons corresponding to the results shown in (B-D). Black framed boxes marked with I, II (1-4), and III (1-3) indicate *5' TPPJ* regions directly bound by WUS – I: -2795 – -2789 bp, II: -2073 – -1830 bp, and III: -652 – -564 bp, as presented in the Figure 3. Grey framed boxes (II5, III3-4, IV1-3, V1, VI1-2) represent *5'TPPJ* regions not directly bound by WUS. (*B-D*) Relative expression of investigated regions (I-III) containing $TPPJ^{WUS}$ elements (I, II1-4, III1-2) in Col-0, *clv3-7* and *clv3-10* (*B*) shoot apex samples without WUS antibody, and (*C*) leaf samples without WUS were used as specificity controls. Please note the amplification in the input and post-binding fractions (PB) and the absence of amplification in the ChIP samples indicating specificity of the antibody used. (*D*) Control overview of all investigated putative $TPPJ^{WUS}$ sites in input and post binding fraction samples. Error bars denote s.d.

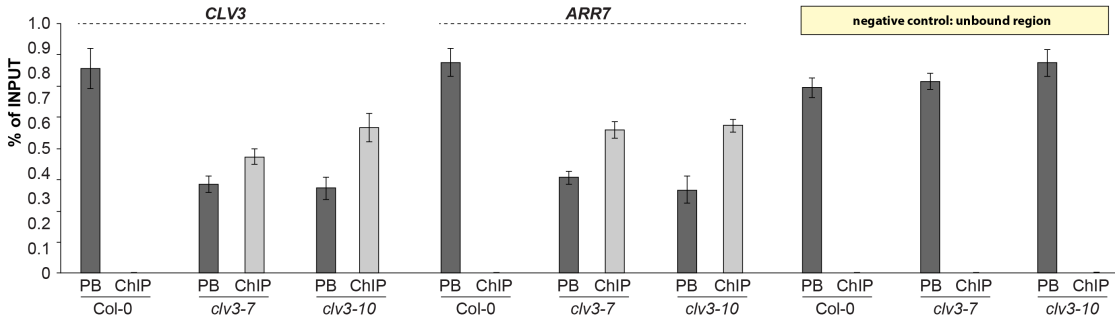

Fig. S12. ChIP-PCR on known WUS targets using a specific WUS antibody. Relative to the input enrichment of known *CLV3*^{WUS} (Yadav *et al*, 2011) and *ARABIDOPSIS RESPONSE REGULATOR 7* (*ARR7*^{WUS}) (Leibfried *et al*, 2005) in *clv3-7* and *clv3-10* as measured by ChIP-PCR. As a negative control a *5'TPPJ* region was used that did not show any WUS binding (unbound region). Error bars denote s.d.

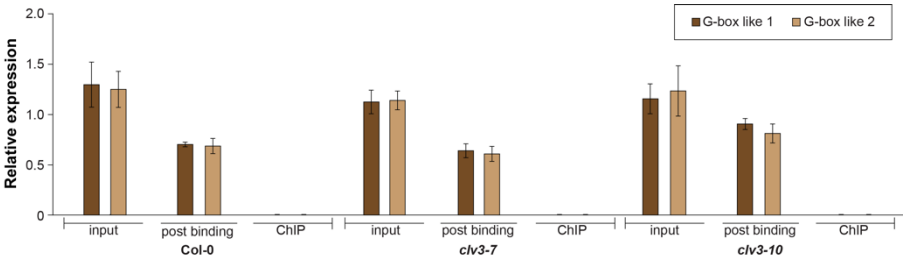

Fig. S13. ChIP-PCR on G-box like WUS binding sites. Relative expression of two G-box like WUS binding regions (CACGTG) (Sloan *et al.*, 2020) present in the *5'TPPJ* intergenic region in input, post binding and ChIP samples of Col-0, *clv3-7* and *clv3-10*. G-box like 1 and G-box like 2 correspond to the regions VI1 and VI2 of Fig. S11A. Please note the amplification in the input and post-binding fractions and the absence of amplification in the ChIP samples. Error bars denote s.d.

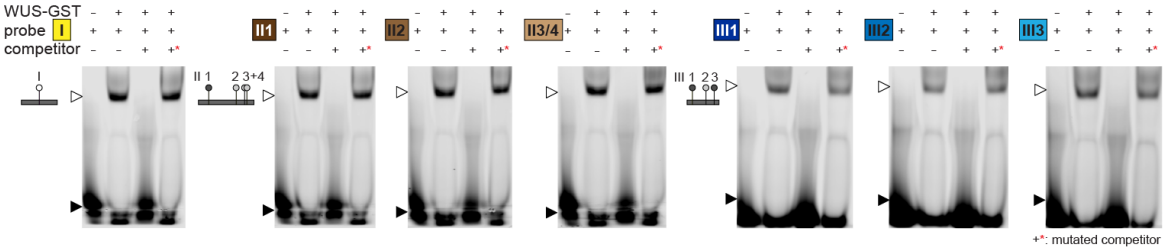

Fig. S14. EMSA control experiments. EMSA for WUS binding to the indicated regions (I-III) in Figure 3A as a control for Figure 3F. Shifted band in the presence of WUS protein (open arrow head), non-shifted fraction (closed arrow head). Please note the shifted band in the presence of the mutated competitor (x*, Table S8) indicating specificity of the binding.

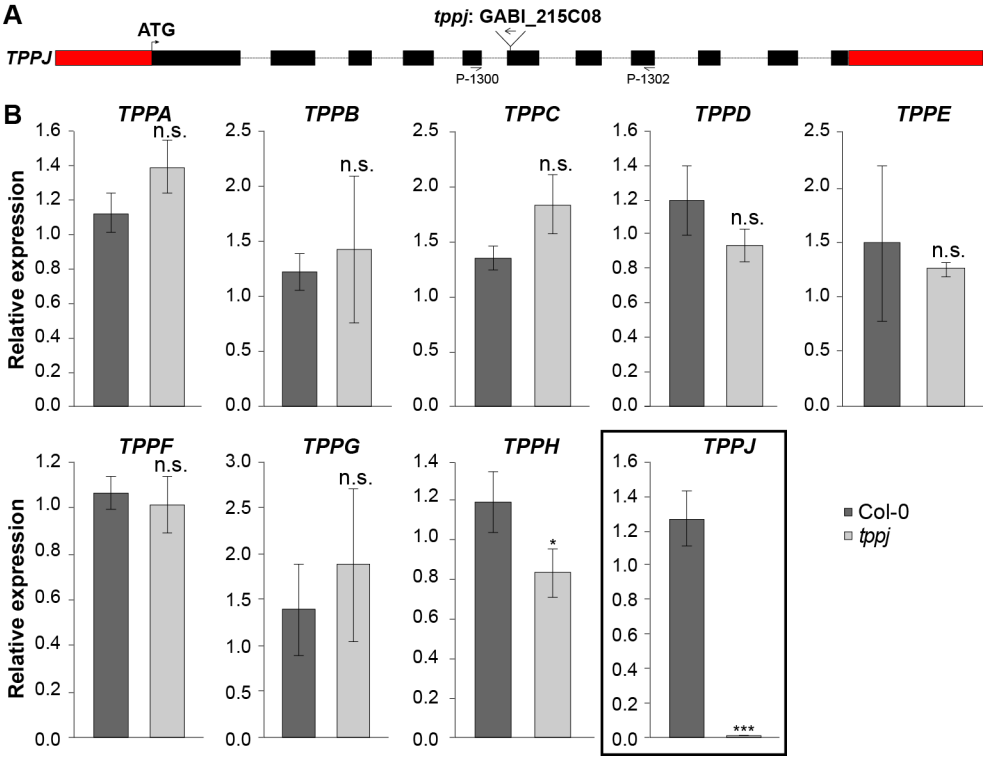

Fig. S15. Chracterization of the GABI_215C08 line. *(A)* Schematic illustration of the T-DNA insertion in the 6th exon of *TPPJ* including positions of oligos used for genotyping. *(B)* Expression of *TPPs* in LD-grown Col-0 and *tppj* rosettes, harvested without roots at 10 days after germination as measured by RT-qPCR. In this experiment *TPPI* was not detectable. Error bars denote s.d.; *P<0.01; ***P<0.001 (one-way ANOVA).

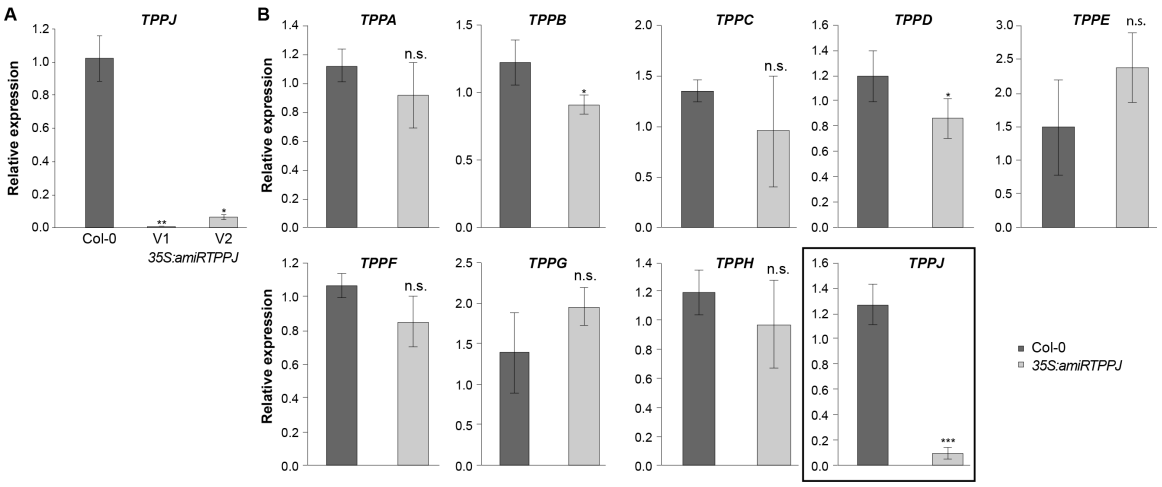

Fig. S16. Characterization of the *35S:amiRTPPJ* lines. *(A)* Downregulation of *TPPJ* expression in *35S:amiRTPPJ* V1 and V2 rosettes shown by RT-qPCR, relative to Col-0. *(B)* Expression of all *TPPs* in LD-grown Col-0 and *35S:amiRTPPJ* V1 rosettes, harvested without roots at 10 days after germination by RT-qPCR. In this experiment *TPPI* was not detectable. Error bars denote s.d.; $^{**}P<0.01$ (one-way ANOVA).

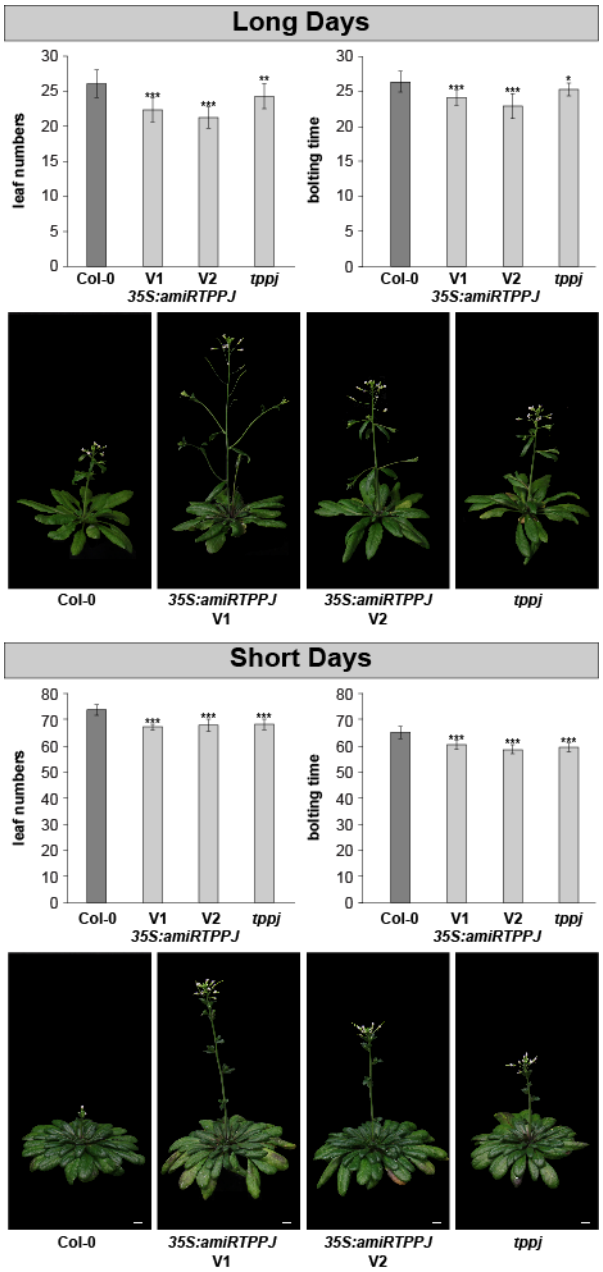

Fig. S17. Earlier flowering of *35S:amiRTPPJ* and *tppj* lines. Flowering time of *35S:amiRTPPJ* V1 and V2 and *tppj* T-DNA insertion line as shown by the total leaf numbers and days to bolting, relative to the wild type in LD and in SD. V1 and V2 indicate two independent versions of artificial microRNAs designed to target *TPPJ* transcript. Representative pictures of *35S:amiRTPPJ* V1 line with stronger reduction in *TPPJ* expression, *35S:amiRTPPJ V2* and *tppj* in comparison to Col-0 are depicted. Scale bars are 1 cm. Error bars denote s.d.; significance calculated based on one way Student's *t*-test; *P<0.05, **P<0.01, ***P<0.001.

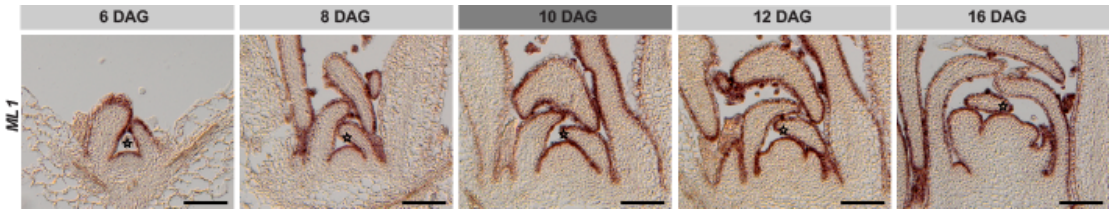

Fig. S18. *ML1* expression throughout development. RNA *in situ* hybridization using a specific probe against *ML1* on longitudinal sections through Col-0 apices from plants grown in LD. 6, 8 DAG depict vegetative SAMs, 10 DAG the transition to flowering, and 12, 16 DAG inflorescence SAMs. Star indicate SAM summit. Scale bars are 100 μm.

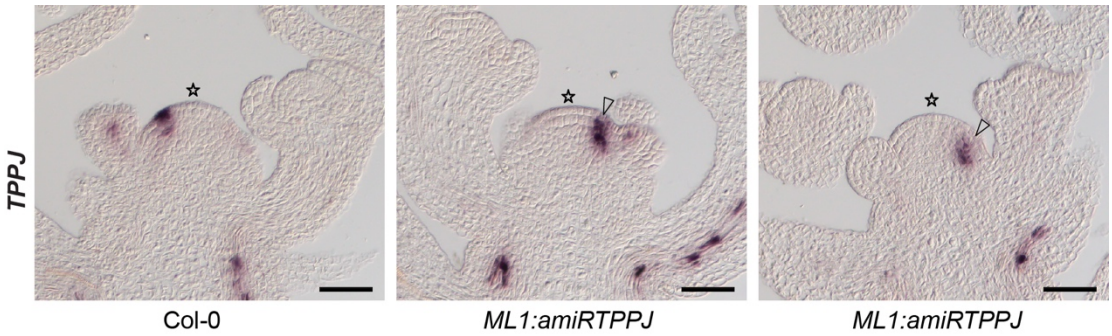

Fig. S19. *TPPJ* expression at the SAM in the background of *ML1:amiRTPPJ* plants. RNA *in situ* hybridization with a specific probe against *TPPJ* did not detect *TPPJ* transcript in L1 (arrow head) on longitudinal sections through SAMs of *ML1:amiRTPPJ* plants (V1). Pictures depict two biological replicates of representative inflorescence SAMs of *ML1:amiRTPPJ* in comparison to Col-0. Star indicate SAM summit. Scale bars are 50 µm.

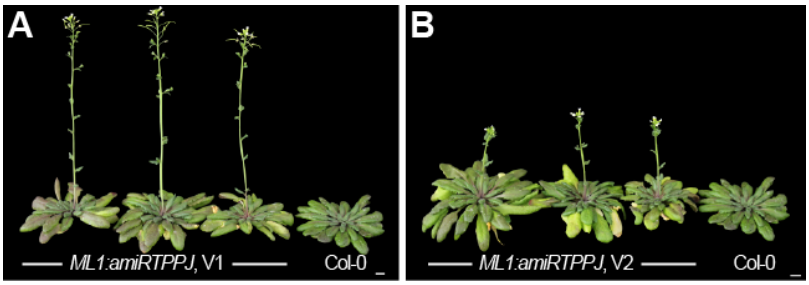

Fig. S20. Early flowering phenotype of *ML1:amiRTPPJ* lines. Representative pictures of (*A*) the stronger *ML1:amiRTPPJ V1* line and (*B*) *ML1:amiRTPPJ V2* in comparison to Col-0 grown in SD conditions. Scale bars are 1 cm.

Fig. S21. Wild-type like flowering phenotype when *ML1:amiRTPPJ* is introgressed into *clv3-10*. Representative pictures of *ML1:amiRTPPJ V1;clv3-10* next to the parental lines and wild type (Col-0) in LD (upper panel) and SD (lower panel) indicating a wild-type like flowering phenotype. Open and closed arrowheads indicate fasciated stem and enormous SAM, respectively. Note the reduced phenotype of the crosses as compared to the *clv3-10* mutant. Scale bars are 1 cm.

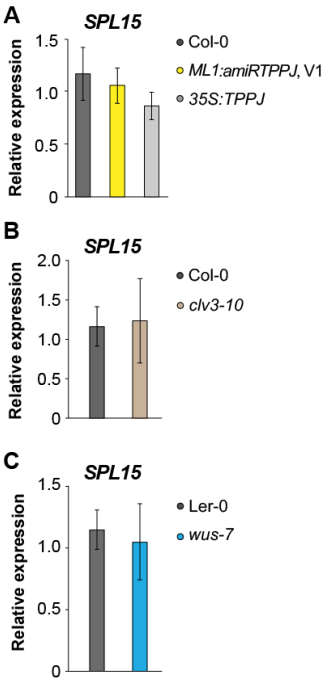

Fig. S22. Expression of *SPL15* at the SAM. *SPL15* does not significantly change at the SAM of (*A*) *ML1:amiRTPPJ* and *35S:TPPJ,* (*B*) *clv3-10*, and *(C) wus-7* compared to its expression in the corresponding wild type. Statistical significance was calculated using one-way ANOVA. Error bars denote s.d.

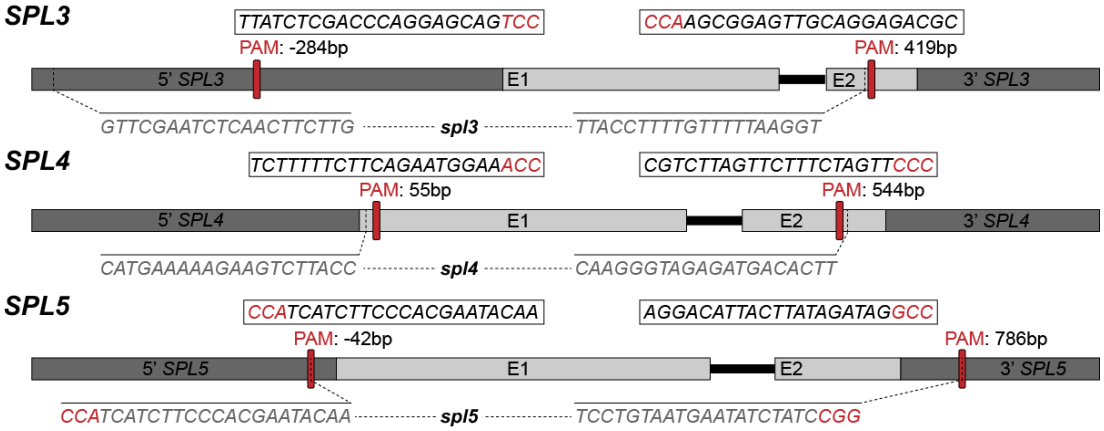

Fig. S23. *SPL3, SPL4,* and *SPL5* mutant lines. Schematic illustration of the deletions in the *SPL3* (At2g33810), *SPL4* (At1g53160), and *SPL5* (At3g15270) locus generated by CRISPR/*Cas9*. Positions of the PAM sequence are given relative to the transcription start site (ATG). Sequences of guided RNAs with PAM sites (in red) are given in white boxes. In grey the sequences flanking the deletion are presented. E – exon.

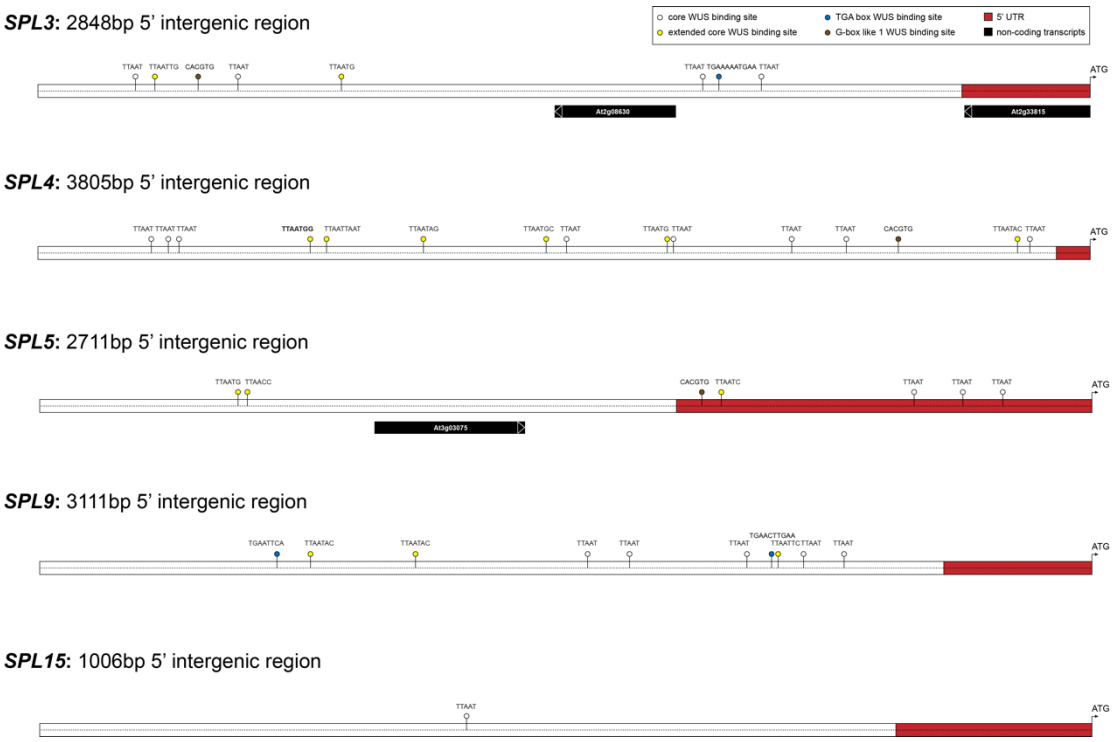

Fig. S24. Potential *SPL*^{WUS} sites in the 5' intergenic regions of *SPL3*, *SPL4*, *SPL5*, *SPL9*, and *SPL15*. Overview of analyses of *SPL3*, *SPL4, SPL5, SPL9* and *SPL15* 5' intergenic sequences for the presence of putative core binding sites (white circles), extended binding sites (yellow circles), TGA boxes (green circles) and G-box-like sites (brown circles). Red boxes indicate *5'UTR*s. Black boxes represent putative transcripts annotated in the intergenic regions upstream the ATG of *SPL3* and *SPL5.* The total sequence lengths are given in base pairs (bp).

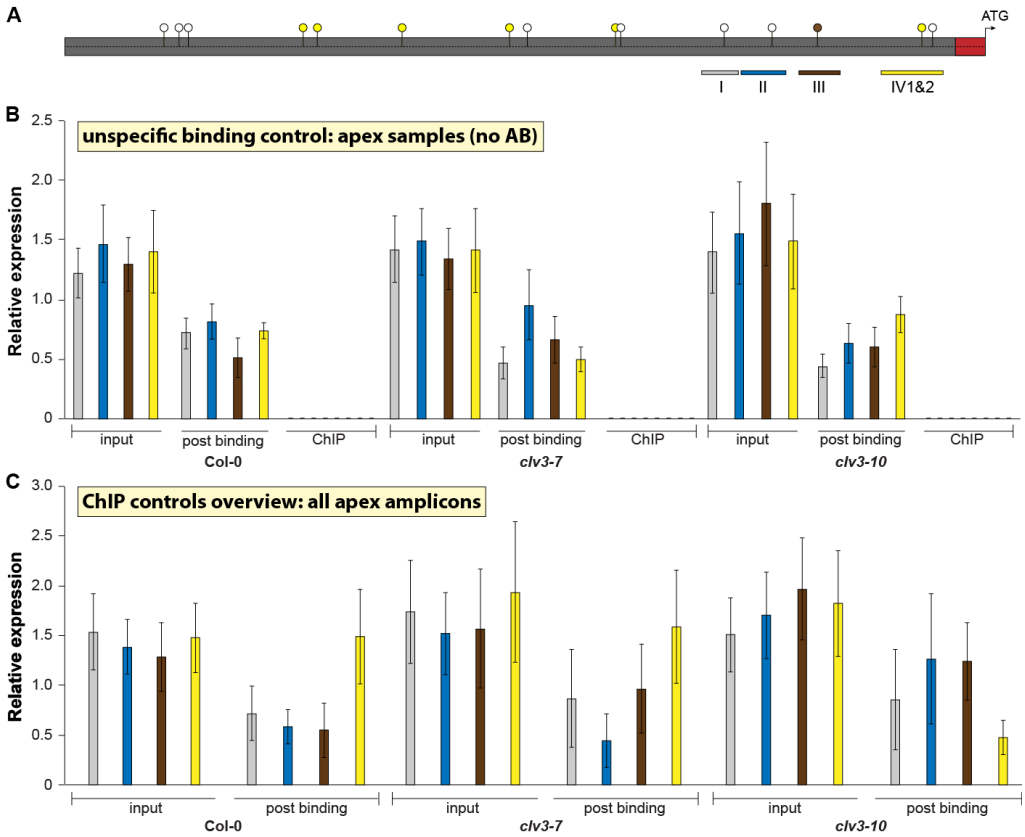

Fig. S25. ChIP-PCR control experiments. (*A*) Overview of 5' *SPL4* intergenic sequence with all investigated putative *SPL4*^{WUS} sites (white, yellow and brown circles), position of ChIP-PCR amplicons corresponding to the results shown in (B and C). Black framed boxes marked with I, II, III, and VI (1&2) indicate *5'SPL4* regions directly bound by WUS – I: -1073 – -1068 bp, II: -880 – -875 bp, III: -697 – -691 bp, and IV: -259 – -209, as presented in Figure 5H. (*B*,*C*) Relative expression of investigated regions (I-IV) containing *SPL4*^{WUS} elements in (*B*) Col-0, *clv3-7* and *clv3-10* shoot apex samples without WUS antibody. (*C*) Control overview of all investigated putative *SPL4*^{WUS} sites in input and post binding fraction samples. Error bars denote s.d.

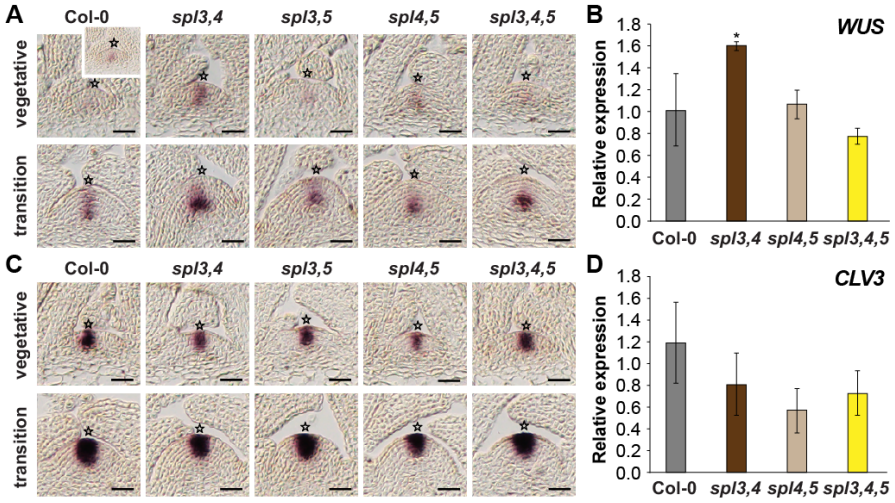

Fig. S26. *WUS* and *CLV3* expression in apices of SD-grown SPL double and triple CRISPR/*Cas9* deletion mutants. Expression provided as (*A,C*) RNA *in situ* hybridization and (*B,D*) RT-qPCR. *WUS* (A,B) and *CLV3* (C,D). n=3. Error bars denote s.d.; significance calculated based on one-way ANOVA; *P<0.05. Scale bars: 25µm. Star indicates SAM summit.

Supplementary Tables S1 to S7

Table S1. Flowering times of Col-0, mutants and transgenic plants. DTF, days to flowering (equals bolting time, see before); RLN, rosette leaf number; CLN, cauline leaf number; TLN, total leaf number; n, number of individual plants; p-value of student's *t*-test for DTF with Co-0; LD, long days; SD, short days; NA, not analyzed (leaf number above 200).

	DTF	DTF range	RLN	CLN	TLN	TLN range	n	p-value
Presented in Figure 4 of the main text:								
Experiment 1 (SD)								
Col-0	71.6	69-75	66.4	11.5	77.9	76-82	20	-
ML1:amiRTPPJ V1 #1	55.0	50-58	49.4	12.0	61.3	58-63	20	3.29E-22
ML1:amiRTPPJ V2 #5	64.4	61-66	52.8	9.2	62.0	60-64	20	3.07E-14
Experiment 3 (SD)*								
Col-0	82.2	79-86	68.6	11.9	80.5	76-86	22	-
ML1:amiRTPPJ V1 #1	65.3	61-69	56.7	9.9	66.5	63-72	22	1.08E-25
clv3-10	95.8	95-101	NA	NA	NA	NA	26	2.17E-25
clv3-10;ML1:amiRTPPJ V1 #1_1	87.3	84-92	NA	NA	NA	NA	24	4.39E-09
clv3-10;ML1:amiRTPPJ V1 #1_3	85.8	82-91	NA	NA	NA	NA	23	4.05E-05
Only presented as supplemental material:								
Experiment 2 (LD)								
Col-0	22.8	22-25	12.1	3.2	15.3	14-16	20	-
ML1:amiRTPPJ V1 #1	20.0	17-21	9.0	3.1	12.1	10-13	20	4.33E-10
ML1:amiRTPPJ V2 #5	21.0	20-22	10.3	2.9	13.2	10-14	20	9.95E-06
Experiment 3 (SD)*								
clv3-7	87.5	85-91	NA	NA	NA	NA	25	1.38E-09
clv3-7;ML1:amiRTPPJ V1 #1_2	74.6	70-78	NA	NA	NA	NA	24	5.50E-22
clv3-7;ML1:amiRTPPJ V1 #1_12	76.9	73-80	NA	NA	NA	NA	24	1.47E-19
Experiment 4 (LD)								
Col-0	26.5	25-29	20.6	5,1	25,7	24-29	31	-
35S:amiRTPPJ V1 #1	24.3	22-26	17.8	4.6	22.3	21-25	32	1.16E-08
35S:amiRTPPJ V1 #2	23.0	21-26	16.8	4.3	21.2	19-23	32	2.24E-11
tppj	25.8	24-28	19.8	4.8	24.6	22-27	35	0.04
Experiment 5 (SD)								
Col-0	65.1	61-68	63.7	10.1	73.7	70-76	30	-
35S:amiRTPPJ V1 #1	60.4	57-62	58.4	9.7	68,1	63-71	30	6.63E-12
35S:amiRTPPJ V1 #2	58.3	56-60	57.8	9.5	67.2	66-69	30	1.47E-17
tppj	59.3	57-62	58.4	9.4	67.8	65-72	30	6.15E-15
Experiment 6 (SD)								
Col-0	72.4	69-75	67.9	9	77.2	74-81	26	-
spl3	73.4	71-75	68.3	10	78.0	75-81	23	0.15
spl4	74.0	71-77	69.2	14	83.0	80-86	26	5.00E-05
spl5	74.0	71-77	68.0	10	77.8	74-82	24	0.45
spl34	77.9	76-80	74.1	17	90.9	87-94	24	5.04E-09
spl35	73.2	71-75	68.4	10	77.9	75-81	24	0.02
spl45	76.8	74-78	73.0	16	76.8	86-93	24	1.25E-11
spl345	84.1	82-87	79.6	19	99.0	94-112	27	2.79E-26

Please note that data marked with an asterisk (*) were obtained from the same experiment.

Table S2. Oligonucleotides for constructs used for the generation of transgenic lines and for transactivation assays.

Gene (AGI)	Oligo	Construct	Sequence (5'→ 3')
TPPJ At5g65140	P-0188	pVW501 *amiRTPPJ V2*	gaTATAATATATCCCCAAGTCGAtctctcttttgtattcc
	P-0189		gaTCGACTTGGGGATATATTATAtcaaagagaatcaatga
	P-0190		gaTCAACTTGGGGATTTATTATTtcacaggtcgtgatatg
	P-0191		gaAATAATAAATCCCCAAGTTGAtctacatatatattcct
TPPJ At5g65140	P-0192	pVW502 *amiRTPPJ V2*	gaTCTAAATGTACTTCACTGCCCtctctcttttgtattcc
	P-0193		gaGGGCAGTGAAGTACATTTAGAtcaaagagaatcaatga
	P-0194		gaGGACAGTGAAGTAGATTTAGTtcacaggtcgtgatatg
	P-0195		gaACTAAATCTACTTCACTGTCCtctacatatatattcct
TPPJ At5g65140	G-8641	pVW279 *35S:TPPJ*	ATGGGTTATGATAATGTATGTG
	G-8642		TTAAACGTTTGGCTTCTTGACAC
5' TPPJ At5g65140	P-1620	pMML049 *5' TPPJ (#1)*	aagggtaccaGAAATACCCTCAAAGCAAATTTGA
	P-1659		CCGTGGCGCGCCCGGTCTTggcgtct
	P-1621	pMML050 *5' TPPJ (#2)*	attggtaccacaGAGTCCACAAGTTTAACAAACAACAGA
	P-1659		CCGTGGCGCGCCCGGTCTTggcgtct
	P-1654	pMML051 *5' TPPJ (#3)*	cttggtaccTTGTCATCATTAAGATGGGATGACA
	P-1659		CCGTGGCGCGCCCGGTCTTggcgtct
	P-1655	pMML052 *5' TPPJ (#4)*	tatggtaccAACGTGGGTGATCATCTCTCG
	P-1659		CCGTGGCGCGCCCGGTCTTggcgtct
	P-1657	pMML054 *5' TPPJ (#5)*	ctaggtaccGTGATTATTGTCAAGGCACCTTAT
	P-1659		CCGTGGCGCGCCCGGTCTTggcgtct
	P-1658	pMML055 *5' TPPJ (#6)*	ttaggtaccCCAAACGAAACAAAAACG
	P-1659		CCGTGGCGCGCCCGGTCTTggcgtct
5' SPL4 At1g53160	P-2040	pMML070 *5'SPL4 (#1)*	ATATGGTACCGCATAAATCCAGATGTTCCTCC
	P-0243		ATATACTAGTCCTTGTCCTTGTGATCTCTTACC
	P-2041	pMML071 *5'SPL4 (#2)*	ATATGGTACCGCTACGGACAAGGTCCTACG
	P-2043		ATATACTAGTCCTTGTCCTTGTGATCTCTTACC
	P-2042	pMML072 *5'SPL4 (#3)*	ATATGGTACCGGCAGCTTTTGGCTTTGG
	P-2043		ATATACTAGTCCTTGTCCTTGTGATCTCTTACC
5' WUS At2g17950	P-2040	pMML067 *5'WUS*	ATATGGTACCGCATAAATCCAGATGTTCCTCC
	P-0243		ATATACTAGTCCTTGTCCTTGTGATCTCTTACC
	P-2041	pMML088 *5'WUS* mutated*	CATGTTCATAA**TTTT**ACCTGTCTTCACAC
	P-2043		GTGTGAAGACAGGT**AAAA**TTATGAACATG
SPL3 At2g33810	P-1334	pMML040 *CRISPR Cas9 SPL3*	accaggtctcaattgAATAGAGCTGGGTCCTCGTCgttttagagctagaaatagcaag
	P-1336		tggtggtctctaaacAGCGGAGTTGCAGGAGACGCcaatctcttagtcgactctacc
SPL4 At1g53160	P-1340	pMMl043 *CRISPR Cas9 SPL4*	accaggtctcaattgGAAAAAGAAGTCTTACCTTGgttttagagctagaaatagcaag
	P-1341		tggtggtctctaaacTTGATCTTTCTTGATTCTGCcaatctcttagtcgactctacc
SPL5 At3g15270	P-1343	pMML027 *CRISPR Cas9 SPL4*	accaggtctcaattgTTGTATTCGTGGGAAGATGAgttttagagctagaaatagcaag
	P-1345		tggtggtctctaaacGATAGATATTCATTACAGGAcaatctcttagtcgactctacc

* Mutagenesis PCR was performed on the pMML067 plasmid. The resulting mutated promoter was sequenced after.

Table S3. Oligonucleotides used for genotyping.

Transgenic line	Oligo	Sequence (5'→ 3')	Position
VW507 *ML1:amiRTPPJ* (V1)	P-0110 P-0189	AGTAGTATGAATTTTCTCTCAC *gaTCGACTTGGGGATATATTATAtcaaagagaatcaatga*	*ML1 promoter* *miRNA stemloop*
VW508 *ML1:amiRTPPJ* (V2)	P-0110 P-0193	AGTAGTATGAATTTTCTCTCAC *gaGGGCAGTGAAGTACATTTAGAtcaaagagaatcaatga*	*ML1 promoter* *miRNA stemloop*
VW504 *35S:amiRTPPJ* (V1)	P-0107 P-0189	AACCTCCTCGGATTCCATTGCC *gaTCGACTTGGGGATATATTATAtcaaagagaatcaatga*	*CaMV 35S promoter* *miRNA stemloop*
VW505 *35S:amiRTPPJ* (V2)	P-0107 P-0193	AACCTCCTCGGATTCCATTGCC *gaGGGCAGTGAAGTACATTTAGAtcaaagagaatcaatga*	*CaMV 35S promoter* *miRNA stemloop*
VW161 *35S:TPPJ*	P-0107 P-0121	AACCTCCTCGGATTCCATTGCC ATTGTGTTCTTCTTCGGAAGAG	*CaMV 35S promoter* *TPPJ* CDS
VW161 *35S:TPS1*	P-0107 P-0120	AACCTCCTCGGATTCCATTGCC ATTATAAGGCCTAACTTCTTGC	*CaMV 35S promoter* *TPS1* CDS
tppj GABI_215C08	P-0208 P-1300 P-1302	TGACCAGCCGCGCTGAATGTG GATGCATCGACAAGGTTTATAGCTTTG GTTACAGTTTTCAAATCCGAGTGACTCTA	*GABI Kat LB* *TPPJ forward* *TPPJ reverse*
*clv3-10**	P-1386 P-1387	TGATGCTTCTGATCTCACTCAAGC CCATTTGCTCCAACCCATTC	*CLV3 forward* *CLV3 reverse*
clv3-7	P-1519 P-1518 P-1387	CCTGAGGTTGGGCAGAAACA TCAAGCTCATGCTCACGTTCA CCATTTGCTCCAACCCATTC	*En-1* LB *CLV3 forward* *CLV3 reverse*
spl3	P-1476 P-1113	GTGGTGTCATAGCAT TGGGAATCAAACGTGACTAGG	*5'SPL3* *3'SPL3*
spl4	P-1498 P-1499	GCTTAACCTATTAGAGTTTC TCGTGGCTCTGAAACTTCAG	*5'SPL4* *3'SPL4*
spl5	P-1497 P-1475	GGAAGCAAGCACATCACGTA CGCAAATAAGAATCAAGTCGAGa	*5'SPL4* *3'SPL4*
Cas9	P-1478 P-1480	CGACCCTCATCCACCAGTCGATTAC CCCAGGCTTTACACTTTATGCTTCC	*Cas9* cassette

*Note that *clv3-10* was genotyped based on sequence analyses.

Table S4. **Oligonucleotides used for RT-qPCR**.

Gene	Oligo	Sequence (5'→3')
TPPJ	P-1300	GATGCATCGACAAGGTTTATAGCTTTG
At5g65140	P-1301	TGAGAAACCTTTAGTTGGGCCTTT
TPPA	P-1493	GATGATCGATAAGGTGCTTTGTTC
At5g51460	P-1494	GCGGTAATGCACAGAGATGC
TPPB	P-1489	CAAGGTAGAAAGGTACTTGAAATCCG
At1g78090	P-1490	ACACCGGCACAACATCATCC
TPPC	P-1487	CAAGGCAGAAAGGTCTTAGAACTCC
At1g22210	P-1488	TCCCTAATGAGTTTAGCAAAAATTCG
TPPD	P-1483	GATGCCGTGATAAGGTTCGTAGAT
At1g35910	P-1484	TGGAAGGTCCTTTGATGTCCA
TPPE	P-1485	CAAGGAAGAAAAGTATTGGAGATTCG
At2g22190	P-1486	ATAGGAAAAACATCGGTACAATTATCA
TPPF	P-1481	ACGCGGGTAGTCATGGAATG
At4g12430	P-1482	CACTTCCTTACCCTGTTGGTCAGT
TPPG	P-1303	GTAAATCCAAATGGATCCCCTGAAG
At4g22590	P-1304	TTACCTCCTCACCCTGTTGGTC
TPPH	P-1495	AGAGTCACTTGGATACGCTAATTGTAC
At4g39770	P-1496	GCCAAGACCTTGTCTTCGTTC
TPPI	P-1482	GCCTTCGCCTCTGTCTCGTA
At5g10100	P-1483	GATGATCGATAAGGTGCTTTGTTC
SPL3	P-1617	GTTTCATGCCAAAGCTCCTC
At2g33810	P-1618	TTTTCCGCCTTCTCTCGTT
SPL4	P-0546	AATGGTCAGGTGGTGATGCAG
At1g53160	P-0547	GCATAGGAAGTGTCATCTCTACCCTT
SPL5	P-0548	CAGCAGGTTTCATGAGCTACCAG
At3g15270	P-0549	CAAAACTGTCACCAGAGATCTTCCTC
SPL9	P-1307	CTTCGCTTTACGAAAATGGTGATG
At2g42200	P-1308	ACTGGCCGCCTCATCACTCT
SPL15	P-1309	CATCTCTTTACGGAAACCCCAATG
At3g57920	P-1310	GCCGCTGCATCACTGATCTT
mir156	P-0342	GCGGCGGTGACAGAAGAGAGT
miRNA universal	P-0343	GTGCAGGGTCCGAGGT
CLV3	P-1386	TGATGCTTCTGATCTCACTCAAGC
At2g27250	P-1387	CCATTTGCTCCAACCCATTC
WUS	P-1382	CCCAGCTTCAATAACGGGAAT
At2g17950	P-1383	ACAGTCTTGTTCCATAGATCCATAGAC
UBQ10	P-0348	CACACTCCACTTGGTCTTGCGT
At4g05320	P-0349	TGGTCTTTCCGGTGAGAGTCTTCA
TUB2	P-0344	GAGCCTTACAACGCTACTCTGTCTGTC
At5g62690	P-0345	ACACCAGACATAGTAGCAGAAATCAAG
SAND	P-0346	AACTCTATGCAGCATTTGATCCACT
At2g28390	P-0347	TGATTGCATATCTTTATCGCCATC
PDF2	P-0350	TAACGTGGCCAAAATGATGC
At1g13320	P-0351	GTTCTCCACAACCGCTTGGT
GAPDH *	P-1125	TCTCGATCTCAATTTCGCAAAA
	P-1126	CGAAACCGTTGATTCCGATTC
At1g13440	P-1127	TTGGTGACAACAGGTCAAGCA
	P-1128	AAACTTGTCGCTCAATGCAATC
miR156 stem-loop **	P-1010	GTCGTATCCAGTGCAGGGTCCGAGGTATTCGCACTGGATACGACG

* Primers used for cDNA quality check according to (Czechowski *et al*, 2004).

** Please note that this oligo was used for cDNA synthesis according to (Varkonyi-Gasic *et al*, 2007).

Table S5. **Oligonucleotides used for ChIP-PCR**.

Gene	Oligo	Region	Sequence (5'→3')
5' TPPJ: At5g65140	P-1624 P-1625	**I**: -3073 bp -2941 bp	GAAATACCCTCAAAGCAAATTTGA AGCTTCTAAAATTCATCAAAACCAA
	P-1628 P-1783	**II (1)**: -2150 bp -1924 bp	GAGTCCACAAGTTTAACAAACAACAGA TCCCATCTTAATGATGACAAACA
	P-1626 P-1782	**II (2)**: -1943 bp -1847 bp	TTGTCATCATTAAGATGGGATGACA TACTGATATATGTTTGCAAAGTTT
	P-1784 P-1627	**II (3+4)**: -1887 bp -1751 bp	TGAATGGAGATAATATAAAACTTTGC TCGAAGACGCCCCTTGTC
	P-1629 P-1630	**II (5)** -1818 bp – 1617 bp	GCCGCTGCTGGTTTTGAG TGTCATTGCATGCATGTGTG
	P-1628 P-1782	**II:** -2150 bp -1847 bp	GAGTCCACAAGTTTAACAAACAACAGA TACTGATATATGTTTGCAAAGTTT
	P-1636 P-1785	**III (1)**: -697 bp -604 bp	CGTGTTCCTATCCATGTTCCT GTATAATGATAAATTTGTAGTAATACC
	P-1786 P-1637	**III (2+3)**: -630 bp -521 bp	GGTATTACTACAAATTTATCATTATAC CCACTTCAACGTTATATCAACCG
	P-1640 P-1641	**III (4)** -826 bp -663 bp	TGTGATTATTGTCAAGGCACCTTAT TTTCATGATTGTATAGGAACATGG
	P-1638 P-1639	**III (5)** -561 bp – 381 bp	CCCCAAACGAAACAAAAACG CCCCGAGCCAAAGGAAAA
	P-1636 P-1637	**III:** -697 bp -521 bp	CGTGTTCCTATCCATGTTCCT CCACTTCAACGTTATATCAACCG
	P-1631 P-1632	**IV (1):** -1353bp -1167 bp	AACGTGGGTGATCATCTCTCG CGTTCAATAGTTGGCACTAAACCA
	P-1633 P-1635	**IV (2):** -1184 bp - 891bp	AGTGCCAACTATTGAACGATTG CGATGCATGCAGCCACAC
	P-1633 P-1634	**IV (3):** -1185 bp – 968 bp	AGTGCCAACTATTGAACGATTG CCATCACGCTCTCGAACTTTCT
	P-1642 P-1643	**V:** -94 bp – 44 bp	TCCTCCTCCTTCCTAGTTTCTCG ATCCCGGTCTTGGCGTCT
	P-2014 P-2015	**VI (1):** -1513 bp – 1387 bp	CCAAAAGGGGACGCGAG TCGATTCCGGTTTCATCGTT
	P-2016 P-2017	**VI (2):** -1513 bp – 1387bp	CGAATACGACGTAGACGAATAAGACA AGCCATGGGACCGAGGTT
5' SPL4: At1g53160	P-2109 P-2110	**I**: -1166 bp -1015 bp	CTTATCTGTTTCCTGCTTTGTTGG CAGTGTGTTGTGTGGAGAAGCA
	P-2111 P-2112	**II**: -1005 bp -821 bp	AGGAAGGTAAAAGTGAGAGGCTTTT GGAGGAATTACAGATTGAAAGATGG
	P-2113 P-2114	**III**: -765 bp -593 bp	GAAAGAAATCAAAAGGGTTAGATCGT TTTGGTAGACTCTTATTGGAAATGCA
	P-2115 P-2116	**IV (1&2):** -425 bp -169 bp	CCTCTTAAAGGCAACCAATGATATC GTGCATGATTACGTTGATGTGC
5' UBQ10: At4g05320	P-1889 P-1890	-582 bp – 306 bp	TCGTGTTTATCAACTCAAAGCACAA TGATCACGGTAGAGAGAATTGAGAGA

Abbreviations: I, **II**, **III (*TPPJ*)** and **I, II, III; IV (*SPL4*)** regions positive in ChIP-PCR, other regions – negative

Table S6. **Oligonucleotides used to prepare constructs for probe synthesis**.

Gene	Construct ID	Oligo	Sequence (5'→3')
WUS: At2g17950	pVW310	P-0148 P-0149	ATGGAGCCGCCACAGCATCAGCATC CTAGTTCAGACGTAGCTCAAGAGAAG
CLV3: At2g27250	pJL102	P-0150 P-0151	TCACTCAGTCACTTTCTCTC GAAAATCATGAGATATAATAG
ML1: At4g21750	pVW510	P-0152 P-0153	ATGTATCATCCAAACATGTTCG TTAGGCTCCGTCGCAGGCCAGAG
TPPA: At5g51460	pVW518	P-0214 G-13892	ATGGACATGAAATCTGGTCACTCGTC TTAACCCATTGATCTCTTCCATGTC
TPPB: At1g78090	pVW516	P-0211 P-0212	ATGACTAACCAGAATGTCATCGTTTC TCACTCTTCTCCCACTGTCTTCCTC
TPPC: At1g22210	pVW515	P-0210 G-13888	ATGAAGATTACGGATATTTCCGGAA TTATTCTCCAAGTGTTTGTTTCTTC
TPPD: At1g35910	pVW257	G-8814 G-8815	ATGACAAACCATAATGCCTTAATC CTATCTTCCTCTTAGTGACATTTG
TPPE: At2g22190	pVW258	G-8816 G-8817	ATGGTTAGATTCATCGAAGAAAATATTAC TCATGCCCCACACCTTGACTGTTTCC
TPPF: At4g12430	pVW227	G-8641 G-8642	ATGGATTTAAACTCAAACCACAAATC TCAAAAACCAGTAGAATTCTTCTCC
TPPG: At4g22590	pVW514	G-8639 G-8640	ATGGATTTGAATATAAACAAGACG TCAAAAACTTGTTTTTGAACTTTC
TPPH: At4g39770	pVW519	P-0215 G-13894	ATGGTTAGATTCATAGAAGAAAACAC TCATGCTCCAGATCTCAATTGTTTCC
TPPI: At5g10100	pVW517	P-0216 P-0213	ATGTCAGCTAGTCAAAACATTGTCG TCACATTCTTGGCTGCATTTGTTTCC
TPPJ: At5g65140	pVW228	G-8641 G-8642	ATGGGTTATGATAATGTATGTG TTAAACGTTTGGCTTCTTGACAC
H4: At2g28740	pAK029	P-0285 P-0286	ATGCTGTTACTTACACTGAGCATG CCAGAAAACCCAGATCTCAAATTG
CYCD3;1: AT4G34160	pVW531	P-0250 P-0251	ATGGCGATTCGGAAGGAGGAAG TTATGGAGTGGCTACGATTGCCC
CDKB2;1 AT1G76540	pVW533	P-0258 P-0259	TGGACGAGGGAGTTATAGCAGTTTC TTAGAGAGAGGACTTTTCTGGCAG

Table S7. **EMSA oligonucleotides (probes) for *5'TPPJ* At5g65140**

Oligo	Modification	Region	Sequence (5'→3')
P-1777 P-1778	5' IR DEY6832	**I**:-2815 bp -2766 bp	ctaaaaattcgttttttttcttaatccggaagataaaaaggttataaaga tctttataacctttttatcttccggattaagaaaaaaaacgaatttttag
P-1779 P-1780	none – competitor	**I**:-2815 bp -2766 bp	ctaaaaattcgttttttttcttaatccggaagataaaaaggttataaaga tctttataacctttttatcttccggattaagaaaaaaaacgaatttttag
P-2186 P-2187	none – mutated competitor	**I**:-2815 bp -2766 bp	ctaaaaattcgttttttttcttcctccggaagataaaaaggttataaaga tctttataacctttttatcttccggaggaagaaaaaaaacgaatttttag
P-1829 P-1730	5' IR DEY682	**II (1)**:-2095 bp -2040 bp	ctattatttttcgctttcaaattaatacacatacaaattaacaaaagta tacttttgttaatttgtatgtgtattaatttgaaagcgaaaaaataatag
P-1841 P-1842	none – competitor	**II (1)**:-2095 bp -2040 bp	ctattatttttcgctttcaaattaatacacatacaaattaacaaaagta tacttttgttaatttgtatgtgtattaatttgaaagcgaaaaaataatag
P-2188 P-2189	none – mutated competitor	**II (1)**:-2095 bp -2040 bp	ctattatttttcgctttcaaattggtacacatacaaattaacaaaagta tacttttgttaatttgtatgtgtaccaatttgaaagcgaaaaaataatag
P-1831 P-1832	5' IR DEY682	**II (2)**:-1922 bp -1878 bp	gacataaaagtcacactgtcaaattaatttgaatatgaatggaga tctccattcatattcaaattaatttgacagtgtgacttttatgtc
P-1843 P-1844	none – competitor	**II (2)**:-1922 bp -1878 bp	gacataaaagtcacactgtcaaattaatttgaatatgaatggaga tctccattcatattcaaattaatttgacagtgtgacttttatgtc
P-2190 P-2191	none – mutated competitor	**II (2)**:-1922 bp -1878 bp	gacataaaagtcacactgtcaaattggtttggtatggatggaga tctccatccataccaaaccaatttgacagtgtgacttttatgtc
P-1833 P-1834	5' IR DEY682	**II (3+4)**:-1863 bp -1814 bp	gcaaacatatatcagtattaattaaatgattaatatgcatttgcagccgc gcggctgcaaatgcatattaatcatttaattaatactgatatatgtttgc
P-1845 P-1846	none – competitor	**II (3+4)**:-1863 bp -1814 bp	gcaaacatatatcagtattaattaaatgattaatatgcatttgcagccgc gcggctgcaaatgcatattaatcatttaattaatactgatatatgtttgc
P-2192 P-2193	none – mutated competitor	**II (3+4)**:-1863 bp -1814 bp	gcaaacatatatcagtattggttaaatgattggtatgcatttgcagccgc gcggctgcaaatgcataccaatcatttaaccaatactgatatatgtttgc
P-1835 P-1836	5' IR DEY682	**III (1)**:-674 bp -625 bp	acaatcatgaaagcttttggttttaatctttttattttattttttggtatt aataccaaaaataaaataaaaagattaaaaccaaaagctttcatgattgt
P-1847 p-1848	none – competitor	**III (1)**:-674 bp -625 bp	acaatcatgaaagcttttggttttaatctttttattttattttttggtatt aataccaaaaataaaataaaaagattaaaaccaaaagctttcatgattgt
P-2194 P-2195	none – mutated competitor	**III (1)**:-674 bp -625 bp	acaatcatgaaagcttttggttttggtctttttattttattttttggtatt aataccaaaaataaaataaaaagaccaaaaccaaaagctttcatgattgt
P-1837 P-1838	5' IR DEY682	**III (2)**:-618 bp -569 bp	aatttatcattatacaactgtacataataatagtagtcatcactatacaa ttgtatagtgatgactactattattatgtacagttgtataatgataaatt
P-1849 p-1850	none – competitor	**III (2)**:-618 bp -569 bp	aatttatcattatacaactgtacataataatagtagtcatcactatacaa ttgtatagtgatgactactattattatgtacagttgtataatgataaatt
P-2196 P-2197	none – mutated competitor	**III (2)**:-618 bp -569 bp	aatttatcattatacaactgtacatggtggtagtagtcatcactatacaa ttgtatagtgatgactactaccaccatgtacagttgtataatgataaatt
P-1839 P-1840	5' IR DEY682	**III (3)**:-585 bp -536 bp	tagtcatcactatacaattaatttccccaaacgaaacaaaaacggttgat atcaaccgtttttgtttcgtttggggaaattaattgtatagtgatgacta
P-1851 P-1852	none – competitor	**III (3)**:-585 bp -536 bp	tagtcatcactatacaattaatttccccaaacgaaacaaaaacggttgat atcaaccgtttttgtttcgtttggggaaattaattgtatagtgatgacta
P-2198 P-2199	none – mutated competitor	**III (3)**:-585 bp -536 bp	tagtcatcactatacaattggtttccccaaacgaaacaaaaacggttgat atcaaccgtttttgtttcgtttggggaaaccaattgtatagtgatgacta

Abbreviations: I, **II**, **III** regions positive in ChIP-PCR.

Table S8. **EMSA oligonucleotides (probes) for 5'*WUS* At2g17950**.

Oligo	Modification	Region	Sequence (5'→3')
P-2172 P-2173	5' IR DEY6832	-1088 bp -1038 bp	gaatactcaacatgttcataagtacacctgtcttcacactcgtttcacac gtgtgaaacgagtgtgaagacaggtgtacttatgaacatgttgagtattc
P-2174 P-2175	none – competitor	-1088 bp -1038 bp	gaatactcaacatgttcataagtacacctgtcttcacactcgtttcacac gtgtgaaacgagtgtgaagacaggtgtacttatgaacatgttgagtattc
P-2180 P-2181	none – mutated competitor	-1088 bp -1038 bp	gaatactcaacatgttcataattttacctgtcttcacactcgtttcacac gtgtgaaacgagtgtgaagacaggtaaaattatgaacatgttgagtattc

SI References

Busch W, Miotk A, Ariel FD, Zhao Z, Forner J, Daum G, Suzaki T, Schuster C, Schultheiss SJ, Leibfried A *et al* (2010) Transcriptional control of a plant stem cell niche. *Dev Cell* 18: 849-861
Czechowski T, Bari RP, Stitt M, Scheible WR, Udvardi MK (2004) Real-time RT-PCR profiling of over 1400 Arabidopsis transcription factors: unprecedented sensitivity reveals novel root- and shoot-specific genes. *Plant J* 38: 366-379
Forner J, Pfeiffer A, Langenecker T, Manavella PA, Lohmann JU (2015) Germline-transmitted genome editing in Arabidopsis thaliana Using TAL-effector-nucleases. *PLoS One* 10: e0121056
Leibfried A, To JP, Busch W, Stehling S, Kehle A, Demar M, Kieber JJ, Lohmann JU (2005) WUSCHEL controls meristem function by direct regulation of cytokinin-inducible response regulators. *Nature* 438: 1172-1175
Schmid M, Davison TS, Henz SR, Pape UJ, Demar M, Vingron M, Scholkopf B, Weigel D, Lohmann JU (2005) A gene expression map of Arabidopsis thaliana development. *Nat Genet* 37: 501-506
Varkonyi-Gasic E, Wu R, Wood M, Walton EF, Hellens RP (2007) Protocol: a highly sensitive RT-PCR method for detection and quantification of microRNAs. *Plant Methods* 3: 12
Wahl V, Ponnu J, Schlereth A, Arrivault S, Langenecker T, Franke A, Feil R, Lunn JE, Stitt M, Schmid M (2013) Regulation of flowering by trehalose-6-phosphate signaling in Arabidopsis thaliana. *Science (New York, NY)* 339: 704-707
Yadav RK, Perales M, Gruel J, Girke T, Jonsson H, Reddy GV (2011) WUSCHEL protein movement mediates stem cell homeostasis in the Arabidopsis shoot apex. *Genes Dev* 25: 2025-2030
Zurcher E, Tavor-Deslex D, Lituiev D, Enkerli K, Tarr PT, Muller B (2013) A robust and sensitive synthetic sensor to monitor the transcriptional output of the cytokinin signaling network in planta. *Plant Physiol* 161: 1066-1075